



HAL
open science

Using natural gas content of groundwater to improve the understanding of complex thermo-mineral spring systems

Margaux Dupuy, Emilie Garel, Eliot Chatton, Thierry Labasque, Alexandra Mattei, Sébastien Santoni, Virginie Vergnaud, Luc Aquilina, Frédéric Huneau

► To cite this version:

Margaux Dupuy, Emilie Garel, Eliot Chatton, Thierry Labasque, Alexandra Mattei, et al.. Using natural gas content of groundwater to improve the understanding of complex thermo-mineral spring systems. *Journal of Hydrology*, 2024, 634, pp.130956. 10.1016/j.jhydrol.2024.130956 . insu-04481433

HAL Id: insu-04481433

<https://insu.hal.science/insu-04481433>

Submitted on 28 Feb 2024

HAL is a multi-disciplinary open access archive for the deposit and dissemination of scientific research documents, whether they are published or not. The documents may come from teaching and research institutions in France or abroad, or from public or private research centers.

L'archive ouverte pluridisciplinaire **HAL**, est destinée au dépôt et à la diffusion de documents scientifiques de niveau recherche, publiés ou non, émanant des établissements d'enseignement et de recherche français ou étrangers, des laboratoires publics ou privés.



Distributed under a Creative Commons Attribution 4.0 International License

Journal Pre-proofs

Research papers

Using natural gas content of groundwater to improve the understanding of complex thermo-mineral spring systems

M. Dupuy, E. Garel, E. Chatton, T. Labasque, A. Mattei, S. Santoni, V. Vergnaud, L. Aquilina, F. Huneau

PII: S0022-1694(24)00350-0
DOI: <https://doi.org/10.1016/j.jhydrol.2024.130956>
Reference: HYDROL 130956

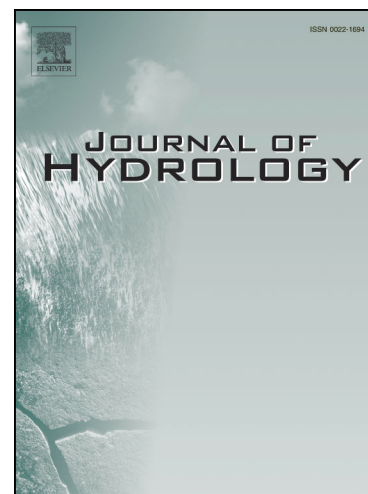
To appear in: *Journal of Hydrology*

Received Date: 5 June 2023
Revised Date: 6 February 2024
Accepted Date: 9 February 2024

Please cite this article as: Dupuy, M., Garel, E., Chatton, E., Labasque, T., Mattei, A., Santoni, S., Vergnaud, V., Aquilina, L., Huneau, F., Using natural gas content of groundwater to improve the understanding of complex thermo-mineral spring systems, *Journal of Hydrology* (2024), doi: <https://doi.org/10.1016/j.jhydrol.2024.130956>

This is a PDF file of an article that has undergone enhancements after acceptance, such as the addition of a cover page and metadata, and formatting for readability, but it is not yet the definitive version of record. This version will undergo additional copyediting, typesetting and review before it is published in its final form, but we are providing this version to give early visibility of the article. Please note that, during the production process, errors may be discovered which could affect the content, and all legal disclaimers that apply to the journal pertain.

© 2024 Published by Elsevier B.V.



1 **Using natural gas content of groundwater to improve the understanding**
2 **of complex thermo-mineral spring systems**

3 M. Dupuy^{1,2,*}, E. Garel^{1,2}, E. Chatton³, T. Labasque³, A. Mattei^{1,2}, S. Santoni^{1,2}, V. Vergnaud³, L.
4 Aquilina³, F. Huneau^{1,2}

5 ¹Université de Corse Pascal Paoli, Département d'Hydrogéologie, Campus Grimaldi, BP 52, 20250 Corte, France.

6 ²CNRS UMR 6134 SPE, BP 52, 20250 Corte, France.

7 ³OSUR - Plateforme Condate Eau, CNRS - Univ Rennes, Géosciences Rennes UMR 6118, 35000 Rennes, France

8 * now at CSIRO, GPO BOX 2583, Brisbane, QLD 4102 Australia (Margaux Dupuy) margauxdupuy@yahoo.fr,
9

10 Abstract

11 The varied gaseous composition of thermo-mineral waters emerging in a non-active
12 zone reflects the diversity and complexity of groundwater pathways and provides
13 important insights into their hydrogeological behaviours. The investigated geochemical
14 content of complex thermo-mineral springs revealed the need to use dissolved gas
15 contents as part of a multi-tracer approach to discriminate processes, geogenic (water-
16 gas-rock interactions), abiotic (geological confinement, flow paths) and biotic activity
17 influencing geochemical of groundwater along regional pathways. Irrespective of the
18 dissolved element content or the water type, examining the overall concentration of
19 dissolved gases enables an effective delineation of regional groundwater flow paths.
20 Using dissolved gas content further contributed to the circumvention of some analytical
21 challenges associated with conventional isotopic or geochemical techniques, often linked
22 to the high concentration of elements such as iron, sulfate, sulfide or other naturally
23 occurring elements content. The primary objectives are to analyse the gas composition of
24 individual springs, to identify the origin of these gases in the groundwater, and to use
25 this gas composition to improve the understanding of the flow patterns contributing to
26 the geochemical diversity observed at the surface of the groundwater. From field
27 investigations in a geologically and structurally complex area of Eastern Corsica (France),
28 three types of gas contents are identified: (type 1) CH₄ & H₂S-rich, (type 2) N₂-rich and
29 (type 3) CO₂-rich. The study of these dissolved gases highlights that the wide geochemical
30 diversity of thermo-mineral waters observed here is not only related to the mineralogical
31 composition of the local aquifer but also involves strong and cumulative interactions
32 along deep regional circulation pathways. This approach also reveals a common deep
33 crustal gaseous influence characterised by N₂ production, which interacts during up flow
34 with groundwater and then with the local metamorphic or sedimentary rock matrix. The
35 groundwater's isotopic and geochemical contents are then altered by local lithologies
36 encountered through both abiotic and biotic interactions. Finally, at shallow depths,
37 phreatic groundwater can add its geochemical and isotopic footprint and dilute this
38 complex mixture before groundwater emerges as mineral spring. This paper answers the
39 primary objectives yet further demonstrates that using dissolved gas as a tracer of
40 groundwater flow paths allows a deeper interpretation of surface geochemical and
41 isotopic observations, distinguishes local from regional flow paths, and provides
42 information about processes at the origin of groundwater diversity.

43 The combination of tools presented in this paper (i.e., geochemical, dissolved gas, and
44 isotopic tools) allows the establishment of a reliable regional groundwater flow scheme
45 for thermo-mineral waters in a non-active zone. This scheme is essential to improve
46 thermo-mineral water management, and protection to ensure their sustainable quality in
47 front of increasing anthropogenic and climatic pressures.

48 **Keywords**

49 Hydrogeology, thermo-mineral waters, water stable isotopes, water-rock interactions,
50 dissolved gases (CO₂, CH₄, H₂S, N₂, He)

51 **1. Introduction**

52 Abundant in thermo-mineral springs, dissolved gases discharged at the surface by
53 groundwaters provide important information about hydrogeological system functioning
54 (Giggenbach, 1991). Widely used as tracers in tectonically active zones in volcanic areas,
55 and seismically-active regions (Werner *et al.*, 2022; Karolytè *et al.*, 2019, 2017; Bräuer *et al.*,
56 2017; Benavente *et al.*, 2016; Ruzié *et al.*, 2013; Mörner and Etiope, 2002), gas emission
57 monitoring is underused as a basis for understanding the hydrogeological functioning of
58 complex hydro-systems that are not linked to an active zone. Some studies reveal that gas
59 discharge could not only be related to regional geotectonic settings but also the result of
60 water-rock interactions or biotic processes occurring through topographical and
61 hydrogeological discontinuities (Lee *et al.*, 2021; Tassi *et al.*, 2020; Kotowski *et al.*, 2019,
62 Agnew and Halihan, 2018; Amaral *et al.*, 2017).

63 As shown by Sacchi *et al.* (2022), to improve the sustainable management of mineral
64 water springs, it is necessary to identify processes occurring along the flow path of
65 valuable springs (i.e. exploited as spa or bottled). For this purpose, geochemical and
66 isotopic tools are the only two tools generally used to characterise mineral waters (Sacchi
67 *et al.*, 2022; Lee *et al.*, 2021; Lavrushin *et al.*, 2018).

68 Nevertheless, the dissolved gas content can provide valuable information about the
69 subsurface flow system by significantly contributing to understanding the origin of flow
70 through the escape mechanisms of natural fluids. Preferential water flow through tectonic
71 structures is responsible for pressure variation, consequently triggering the progressive
72 release of gas at the surface as a function of their solubility. In the non-active zone, some
73 studies have revealed that gas-rich waters are only generated by meteoric water
74 infiltration and groundwater rocks interactions even in the shallowest part of the crust
75 (Agnew and Halihan, 2018). Subject to the natural increase in temperature with depth,
76 waters are warmed and, then flow through and between geotectonic units. The latter are
77 preferential pathways that allow water to quickly reach the surface before losing heat
78 (Goswami *et al.*, 2022; Craw *et al.*, 2013; Grasby *et al.*, 2000). Physical and chemical
79 alterations due to depth associated with geological and geotectonic conditions can
80 increase water rock interactions and lead to gas release (Štrbački *et al.*, 2020). From the
81 respective proportions of dissolved carbon dioxide (CO₂), methane (CH₄) or nitrogen (N₂)
82 combined with the proportion of reactive (H₂, H₂S, etc.) or noble (He, Ne, Ar) gases
83 measured in groundwater, processes causing their release could be identified (Agnew and

84 Halihan, 2018). Apart from atmospheric origin, the dissolved CO₂ has various origins such
85 as deep-seated mantle (magmatic influence), thermogenic or biogenic (both occurring in
86 sediments). Well known as anthropogenic emission (i.e. landfill, agricultural activities,
87 etc.), the greenhouse gas CH₄ has multiple natural origins such as volcanic and, wetlands
88 and or could be also the evidence of biotic processes from an anaerobic environment
89 where microbial fermentation of organic matter occurs. The last major gas found is N₂,
90 which may have an atmospheric origin, a magmatic origin, or can be caused by the
91 intrusion of deep fluid. According to their potential origin and to their geochemical and
92 isotopic composition, groundwater samples collected at the surface can provide
93 information about fluid origin, up-flow paths and reservoir interactions with geological
94 matrixes (D'amore *et al.*, 1987). To ensure the sustainability of this mineral groundwater,
95 gas monitoring was revealed to be a powerful and innovative tool to identify
96 hydrochemical processes at the origin of springs, and to conceptualise the whole
97 hydrogeological system as well as the aquifer conditions of flow paths. This study aims
98 to use dissolved gases as integrative tracers of the water pathways within a non-active
99 zone and regardless of the geological context or geological unit encountered (Marques *et*
100 *al.*, 2020; 2000 Tassi *et al.*, 2020; Angelone *et al.*, 2005; Minissale *et al.*, 2019, 2004, 1999;
101 Michard, 1990).

102 Corsica Island (France), and particularly its eastern part, highlights a wide
103 hydrochemical diversity of thermo-mineral waters (Na-HCO₃, Ca-HCO₃, Ca-SO₄- HCO₃
104 and Na-Cl), not linked to any seismic- or tectonic activity (Dupuy *et al.*, 2021). Emerging
105 from a small mountain-plain continuum (<16 km), at the interface of sedimentary,
106 metamorphic and igneous rocks, eastern Corsica thermo-mineral groundwater diversity
107 is evidence of the existence of complex flow patterns and thus a perfect site for detailed
108 investigations on groundwater gaseous content. To improve the gap in knowledge
109 regarding the origin of the gas diversity observed, noble gases (He, Ne, Ar) and reactive
110 gases (CO₂, N₂, H₂S, CH₄, H₂, O₂) were monitored to test the potential of dissolved gases
111 to improve the hydrogeological understanding of 22 mineral springs.

112 The main aims were (1) to describe the gas composition of each spring; (2) to
113 characterise the origin of these gas phases in groundwater and to differentiate geogenic
114 from biotic influences. Then, using this gas composition (3) improves the description of
115 the flow patterns involved in the groundwater diversity observed at the surface.

116 This work provides significant information regarding the major interest in
117 investigating the gaseous phases of groundwaters in non-active zones, taking advantage
118 of the complex hydrogeological model offered by Corsica Island geological conditions.

119 2. Study area

120 Localisation and hydroclimatology

121 In the Western Mediterranean Sea, Corsica Island (France) has a contrasted topography
122 (up to 2706 m. above sea level – asl.). The investigated area, located on the eastern part of
123 the island extends over 1,500 km². In the west of the study area, a mountainous zone, of
124 1034 km², rises to 2136 m, while in the east, the coastal part is a lowland plain extending
125 over 466 km². Despite the typical Mediterranean climate of the island, the mean
126 temperatures and precipitation vary significantly with the altitude (Fig. 1). According to
127 Bruno *et al.* (2001) average annual precipitation increases from about 600 mm near the
128 coast to more than 1600 mm at 1500 m asl, while the mean annual temperature decreases
129 from 16°C near the coast to 10°C at 1500 m asl (Mattei *et al.*, 2021; Bruno *et al.*, 2001). These
130 observations are confirmed by the ombrothermal diagrams displaying precipitation and
131 temperature observed on 3 cities of the study area, at Corte at 429 m asl (inland), Bastia
132 and Solenzara, two lowland stations respectively at 1 and 12 m asl . The inland part is
133 characterised by alpine climate conditions with high snowfall in winter and storm rain
134 events during the driest months from May to September for inland stations (Fig. 1) (Mattei
135 *et al.*, 2021; Rome and Giorgetti, 2007). While lowland stations saw their driest months
136 from April to September (Fig. 1). The study area is drained by four main rivers flowing
137 from West to East: the Solenzara River and the Travu River in the south part, the
138 Tavignanu River and the Golu River in the northern part (Fig. 2).

139 Geological and hydrogeological overview

140 The study area is located at the interface of 4 main geological units on the island (Fig.
141 2) (Caritg, 2009a, 2009b). The basement, mainly made of calc-alkaline granitoid rocks from
142 the Hercynian orogenesis, extends over the south-west. It is overlapped, along an N.NW-
143 S.SE axis, by two units from the Alpine orogenesis; the first unit is Eocene flysch, an
144 autochthonous sedimentary detrital unit and the second is lustrous schists, an
145 allochthonous metamorphic unit also called 'Alpine metamorphic unit', observed only in
146 the 'Castagniccia region'. The Neogene sedimentary basin of the Aleria plain is separated
147 from the allochthonous units by the Saint Antoine fault N.NE-S.SW oriented (N020°)
148 (Loÿe-Pilot *et al.*, 2004). Geological and hydrogeological information of each unit
149 encountered in the study area is detailed in the paragraphs below.

150 In the study area, the Hercynian basement is mainly composed of biotite-rich
151 monzogranite, tonalo- or monzogranodiorite (Rossi *et al.*, 2015; Caritg, 2009a, 2009b). The
152 Pietrapola springs (Fig. 2) flow out of monzogranite in which alkaline feldspar [Na, K]
153 and plagioclase dominate [Na, Ca]. In the Travu valley, the Caldaniccia spring (Fig. 2)
154 flows out of tonalogranodiorite and monzogranodiorite, with plagioclase feldspars
155 dominant over alkaline feldspars, biotite [K, Mg, Fe, F] and amphibole [Ca, Mg, Fe]. The
156 granitic basement is intensively fractured by NE-SW faults (Caritg, 2009a). Only a few

157 reports from the French geological survey exist and they provide basic information on
158 groundwater flows and aquifer capacity of this unit (Caritg, 2009a, 2009b). As in a mainly
159 hard rock context, deep fractures associated with the superficial weathered horizon are
160 the most favourable zones for the groundwater circulation and aquifer capacity
161 (Lachassagne, 2011; Genevier *et al.*, 2011; Dewandel *et al.*, 2011; Caritg, 2009a; Caballero *et*
162 *al.*, 2006).

163 The Alpine metamorphic units are derived from the exhumation of oceanic and
164 continental tectonic units involved in the Alpine orogeny (from the Late Cretaceous to the
165 late Eocene, *e.g.*, (Di Rosa *et al.*, 2017). These tectonic units include metamorphic granitoids
166 and metamorphic sedimentary rocks with metamorphic rocks derived from the oceanic
167 crust (serpentinites, metagabbros and metabasalts). The observed so-called 'Lustrous
168 schists' display a wide range of metamorphic facies from blueschist facies (mainly Inzecca
169 series), eclogite facies (mainly Serra di Pigno and Castagniccia series) to greenschist facies
170 (Piccoli *et al.*, 2018; Gueydan *et al.*, 2017; Di Rosa *et al.*, 2017; Vitale Brovarone *et al.*, 2013;
171 Caritg, 2009b). These units are intensively folded and characterised by discontinuities
172 displaying an NS orientation of schistosity, creating favourable hydrogeological
173 conditions for many springs in the Castagniccia region (Fig. 2).

174 The Eocene autochthonous flysch is a vertical alternation of conglomerates, sandstones
175 and dark clay, mainly made of arkose and pelite rocks. This formation rubs up against the
176 Hercynian basement along the NE-SW contact and is overlapped by sedimentary deposits
177 in the eastern part (Berthier *et al.*, 1980; Amaudric, 1973). Vignola springs from the Travu
178 Valley, Fontanella and Acqua acetosa are springs flowing out at the interface of this
179 heterogeneous unit known as a low aquifer potential area (Caritg *et al.*, 2009b).

180 The Neogene sedimentary formation is heterogeneous: from breccias and
181 conglomerates to sands and marls. Due to basin subsidence, Neogene deposits dip to the
182 east with an approximate thickness of 2 km at the coastline and up to 8.5 km in the middle
183 of the Corsican channel. Covered by thin Quaternary alluvial deposits (Fig. 2), they are
184 cut by N145-N155 and N20-N30 faults. These Neogene sediments present a few shallow
185 local aquifers with very low productivity. However, their thickness and lithologic
186 diversity suggest a noticeable hydrogeological potential as a deep multi-layer aquifer
187 supported by the occurrence of artesian boreholes (Serrano *et al.*, 2013; Loÿe-Pilot *et al.*,
188 2004).

189 Hydrochemical background of springs in the study area

190 Twenty-four thermo-mineral springs flow out at the interface of the main geological
191 formations described above (Fig. 2). Dupuy *et al.* (2021) the 6-month sampling campaign
192 in 2018 provides a first overview of hydrochemical characteristics of 19 thermo-mineral

193 groundwaters and results are summarised below.

194 The Pietrapola and Caldaniccia sites show springs flowing out respectively from
195 potassium feldspar-rich- monzogranite and tonalogramiodiorite. Thereby a high-altitude
196 recharge (>800 m asl) supplies the springs emerging through major faults providing
197 thermal-alkaline-water, fully equilibrated with rock. Their low mineralisation (<300
198 $\mu\text{S}/\text{cm}$) associated with a Na-HCO₃ water type and high SiO₂ content confirms that this
199 water is provided by the hydrolysis of Hercynian granitoids at depth (Dupuy *et al.*, 2021).

200 All other springs are cold resulting from a local recharge at a shallower depth. Acqua
201 acetosa, Vignola and Fontanella flow out at the interface between Eocene Flyschs and
202 Hercynian basement or Neogene sediments (Table 1). These 3 springs are highly
203 mineralised (from 2100 and up to 12 000 $\mu\text{S}/\text{cm}^2$), contain high levels of chlorine, boron
204 and fluorine and display respectively a Ca-Na-HCO₃ for Acqua acetosa and a Na-Cl water
205 type for the latter two. Their high mineralisation comes partly from the dissolution of
206 interstitial-residual-brines (Aquilina *et al.*, 2011). This geochemical diversity translates to
207 the importance of tectonics in the complexity of the flow pattern involved at the interface
208 of the different geological units (Martín-Loeches *et al.*, 2020).

209 The Puzzichellu springs group flows out along the Saint Antoine fault, aligned on a
210 N20-N30 axis (Fig. 2), where the Puzzichellu and the Campo-Favajo springs emerge from
211 sandstones including rhyolite conglomerates covered by deposits of organic matter-rich
212 marls (Caritg *et al.*, 2009a, 2009b). This group is characterised by Na-HCO₃, Ca-Na-HCO₃
213 and Ca-SO₄- HCO₃ water types. Here, deep groundwaters are influenced during the
214 upflow process by mixing with more carbonated groundwaters of sedimentary origin
215 (Dupuy *et al.*, 2021). The sulfur isotopes performed on the artesian borehole of the
216 Puzzichellu site (PUZ-F, Table 1) have shown the presence of bacterial activity, explaining
217 the high sulfate and sulfite content recorded in the groundwater (Dupuy *et al.*, 2021;
218 Dominici *et al.*, 1986).

219 3. Sampling and analytical procedures

220 3.1. Sampling strategy and rainfall data

221 Based on their legal accessibility, geology and spatial coverage 22 thermo-mineral
222 waters, located at 15 different sites and flowing out at low altitudes (<554 m asl) were
223 sampled. The location, name and exact geographical coordinates are provided in Table 1.

224 To identify altitude recharge of precipitation at a regional scale, $\delta^{18}\text{O}$ and $\delta^2\text{H}$ extracts
225 from a monthly sampled precipitation observation network at 5 stations [Aleria (9 m),
226 Bastia (1 m), Bonifacio (99 m), Corte (486 m), Campana (760 m), and Palneca (785 m)] were

227 used to calculate the isotopic altitudinal gradient from data extracted from Nlend B. *et*
228 *al.*(2023)and Mattei *et al.* (2021). By calculating the linear regression relating the rainwater
229 stable isotope values to their sampling altitude, a regional isotopic elevation gradient can
230 be obtained; here considered equal to $\delta^2H = -0.019 * altitude (m\ asl) + (-34.876)$. This
231 equation can be used to estimate the recharge altitude of springs out on the eastern part
232 of the island.

233 3.2. Groundwater sampling procedures

234 The 22 springs were sampled monthly from January 2018 to March 2019. Physical and
235 chemical parameters were simultaneously measured in the field. Electrical conductivity
236 (EC), temperature (T), redox potential (Eh) and pH were measured with a WTW multi
237 3410 (WTW gmbH, Weilheim, Germany). Bicarbonates concentration (HCO_3) was also
238 determined, in the field, using a HACH digital titrator (HACH Company, Loveland,
239 USA). Samples were filtered through 0.45 μm nitrocellulose membranes for
240 determination of major ions and stored in two 50 mL polyethylene bottles before storage
241 at 4°C. One bottle was acidified using ultrapure nitric acid for cation analysis. A Dionex
242 ICS 1100 chromatograph (Thermo FischerScientific, Waltham, USA) was used to
243 determine ionic concentrations at the Hydrogeology Dept. of the University of Corsica
244 (CNRS UMR SPE 6134). The analysis was checked and validated for ionic balance under
245 10%.

246 For the stable isotopes of the water molecule analysis ($\delta^{18}O/{}^2H$), 20 mL amber glass
247 bottles were filled without filtration and no headspace to ensure perfect conservation then
248 were stored at 4 °C. They were determined using a Liquid-Water stable isotope analyser
249 DLT-100 (Los Gatos Research, San Jose, CA, USA) at the Hydrogeology Department of
250 the University of Corsica (CNRS UMR 6134), France, following the analytical scheme
251 recommended by the IAEA (Penna *et al.*, 2010). The analytical precision was better than
252 0.5‰ for 2H and 0.2‰ for ${}^{18}O$.

253 For tritium (3H) analysis, 500 ml polyethylene bottles were filled and then stored at 4°C
254 until analysis. The 3H activity was measured by a liquid scintillation analyser (DL > 0.2
255 UT) following the protocol of Thatcher et al (1977). These analyses were carried out at the
256 Hydrosys Labor Kft. in Budapest, Hungary.

257 3.4. Gas sampling procedures

258 During four campaigns in 2018 (April, July, September, and December), springs were
259 also sampled for the analysis of dissolved gases in 500 ml glass bottles by over-flushing,
260 after rinsing three times the bottle volume with the spring water. Bottles were closed with
261 rubber caps and sealed with a metal ring, then sent within 48 hours for analyses at the

262 Geosciences Rennes laboratory (CNRS UMR 6118) as detailed in Chatton *et al.*, 2017.
263 Noble and reactive gases (Ne, He, Ar, N₂, O₂, CO₂) were extracted by headspace and
264 measured by gas chromatography equipped with a catharometer detector (μ GC 3000 –
265 SRA) at the Condate Eau platform (OSUR CNRS - Univ Rennes, France). Uncertainty is
266 estimated at +/- 5% for [CO₂] and [CH₄] and +/- 3% for other gases.

267 The anthropogenic gases (CFCs and SF₆) were sampled in stainless-steel ampoules after
268 washing through at least three volumes of the ampoule and before closing it to ensure no
269 air contamination. Their concentrations in groundwater were obtained through a
270 methodology of purge-and-trap inspired by Busenberg et Plummer (1992). Water was
271 degassed by N₂ stripping and gases were trapped in a stainless-steel tube filled with
272 HayesepD® and maintained at -100 °C in an ethanol bath. After 6 (CFCs) or 10 (SF₆) min
273 of pre-concentration, the gases were injected into a Gas Chromatograph equipped with
274 an Electron Capture Detector (GC-ECD, Perkin Elmer) by immersing the trap into boiling
275 water. The analytical uncertainty is estimated to be 1–3% for CFCs and near 5% for SF₆.
276 Analyses were performed at the Condate Eau Platform (OSUR CNRS-Univ Rennes,
277 France).

278 3.5 Recharge condition modelling

279 Dissolved gases, such as argon (Ar), nitrogen (N₂) and neon (Ne), were used to model
280 recharge conditions, using an inverse model developed from the methods described by
281 Aeschbach-Hertig *et al.* (1999). This model has been adapted to use the available dissolved
282 Ne, Ar and N₂ concentrations in cm³STP/g (Standard Temperature and Pressure) to model
283 the Temperature (NGT) and the amount of excess air (EA) as already applied on
284 hydrogeological systems by Chatton *et al.* (2017). Limited by the low quantity of available
285 dissolved gases (Ne, N₂ and Ar) and their related analytical uncertainty, this study
286 considers a simple model of excess air formation to determine the recharge conditions
287 (NGT and EA). The established inverse model is established considers an Unfractionated
288 Air model (UA model), which assumes a total dissolution of unfractionated excess air
289 during the recharge. That means that the reverse model will consider that dissolved noble
290 gas concentrations depend on different parameters: the recharge temperature (so-called
291 noble gas temperature, NGT), the volume of unfractionated excess air (EA), the altitude
292 of recharge and the recharge salinity. The two latter field parameters being known, only
293 two free parameters (NGT and EA) remain to be determined using the inverse model with
294 a degree of freedom $\nu = 1$. Because absolute NGT values were not conclusive, only the
295 Excess Air (EA) concentration was used in this paper and results are displayed in Table 3.

296 297 3.6 Statistical analysis: Principal component analysis (PCA) and Hierarchical clustering 298 (HCA)

299 A Principal Component Analysis (PCA) is a statistical technique used for a
300 dimensionality reduction of input data in order to simplify data visualisation. In our
301 study, PCA is applied to identify patterns and relationships within complex datasets of
302 variables such as physicochemical parameters (pH, Eh, T, E.C), geochemical components
303 (HCO_3) and gas contents (O_2 , CO_2 , CH_4 , H_2S , N_2 , He, Ne, Ar, H_2) and displaying it by
304 springs. It allows us to represent the data in a lower-dimensional space, facilitating the
305 interpretation of underlying patterns (Everitt, B.S., 2001, Kim, K.-H, 2020).

306 A heatmap generated by Hierarchical Cluster Analysis (HCA) visually represents the
307 results of clustering analysis. In the context of HCA, a heatmap displays a matrix of
308 colours where each cell corresponds to a pair of variables or observations. The intensity
309 of the colour in each cell indicates the degree of similarity or dissimilarity between the
310 paired variables or observations. Clusters of similar entities are visually apparent as
311 contiguous blocks of similar colours, providing a clear representation of hierarchical
312 relationships within the dataset. Heatmaps are valuable for identifying patterns, trends,
313 or groupings in complex datasets analysed through HCA. In our study, according to the
314 methodology displayed by Tarvainen (2019), HCA is employed to categorise gas
315 abundance in springs into hierarchical structures, aiding in the identification of distinct
316 groups within the dataset.

317 4. Results and discussion

318 4.1. Water type diversity

319 During the sampling period, the groundwater temperature ranges from 11 to 54°C
320 distinguishing thermal waters ($T > 20^\circ\text{C}$), such as at the Pietrapola site and the Travu valley
321 ($N = 8$), from cold waters ($T < 20^\circ\text{C}$) which concerns all the other springs ($N = 14$, Table 1).
322 A wide range of mineralisation levels and pH values are observed ranging from 150
323 $\mu\text{S}/\text{cm}$ (CALD) to 12 620 $\mu\text{S}/\text{cm}$ (FONT) with pH ranging between 4.45 (S-SUP) to 9.7 (P-
324 LAV) (Table 2). In order to discriminate water types, major element proportions were
325 displayed on a Piper diagram (Fig. 3). Three main water types are observed Na-Cl, Na-
326 HCO_3 and Ca- HCO_3 , also with two intermediate facies Na-Ca- HCO_3 and Ca- SO_4 - HCO_3 .
327 Thermal waters at the Pietrapola site and CALD, show a typical Na- HCO_3 water type
328 affirming their geothermal origin from granitoid rocks (Fig. 2) (Martín-Loeches *et al.*,
329 2020). The thermal spring VIGN and the cold spring FONT, have a Na-Cl water type; this
330 mature water (Giggenbach, 1988) shows long-time interaction with detrital rocks. The Ca-
331 HCO_3 water type is observed for all the Castagniccia Region springs (Fig. 2, 3) except S-
332 SUP, which displays an intermediate Ca- SO_4 - HCO_3 water type, PORT and FAJO-G
333 displaying another intermediate facies Na-Ca- HCO_3 .

334 Springs located on the sedimentary plain show diversified water types: CAM-F with a

335 Na-HCO₃ water type is close to waters flowing through granitic rocks; ACQ has an
 336 intermediate facies Na-Ca-HCO₃ characteristic of groundwaters flowing at the interface
 337 of magmatic and sedimentary rocks (Martín-Loeches *et al.*, 2020); then the Puzzichellu site
 338 shows two springs with another intermediate Ca-SO₄-HCO₃ water type.

339 Thus, the geochemical signature of the thermo-mineral springs highlights five different
 340 groundwater types, representing a high diversity of springs for a small area. These five
 341 water types (Fig. 3) and their spatial distribution (Fig. 2) are not correlated with the
 342 geological unit from which they spring out.

343 4.2. Water gas composition

344 4.2.1. Multi-criteria classification of gaseous discharge

345 To improve the understanding of groundwater flows and to discriminate the origin of
 346 the various geochemical signatures, a multi-criteria classification of gaseous discharge
 347 composition was carried out by applying hierarchical cluster analysis (HCA) on chemical
 348 abundance gas measured in April, September and December 2018 (Table 3). In Fig. 4, the
 349 average gas concentration by spring is depicted according to colour from low
 350 concentration (dark blue) to high concentration (deep red). Hierarchical cluster analysis
 351 is performed on the 13 thermo-mineral groundwater samples, based on 9 dissolved gas
 352 components (Ne, He, Ar, N₂, H₂, CO₂, O₂, CH₄, H₂S) and indicates the existence of only
 353 three clusters with three distinct gaseous types: Type I (CH₄ and H₂S), Type II (N₂) and
 354 Type III (CO₂). Visual inspection of the vertical dendrogram reveals that cluster 1 is linked
 355 to the remaining two other cluster types at a great distance, indicating that the gaseous
 356 origin of Type I differs strongly from the rest of the analysed groundwater. Each related
 357 cluster and main gas composition is detailed below.

358 4.2.1.1 Type I: CH₄ and H₂S rich springs

359 Cluster 1 concerns a borehole (PUZ-F) and a natural water spring (CAM-F) flowing
 360 out from the Neogene sedimentary depositions (Fig. 2). These groundwaters are
 361 intermediately mineralised (1041 < E.C. < 1592 μS/cm), neutral to alkaline (6.9 < pH < 8, mean
 362 value 7.3), with varying water types due to major ions showing natural variations (Fig. 3):
 363 from Ca-HCO₃-SO₄ in PUZ-F to Na-HCO₃ in CAM-F. Temperatures are below 20°C (13.5 <
 364 T(°C) < 17.5) and a typical smell of hydrogen sulfide (rotten egg) is very strong at both
 365 sites. Springs concerned by the Cluster I are characterised by the highest concentration in
 366 CH₄ and H₂S measured in the study area with an average CH₄ concentration of 9*10⁻⁴ mol/l
 367 (PUZ-F) up to 2*10⁻³ mol/l (CAM-F) and an average H₂S concentration of 1*10⁻⁴ mol/L
 368 (PUZ-F) to 4*10⁻⁵ mol/l (CAM-F) (Table 3, Fig. 4). The average H₂ content (1*10⁻⁸ mol/l)
 369 measured in CAM-F is noticeable. The average CO₂ content varies from 1*10⁻³ to 3*10⁻⁴

370 mol/l, for CAM-F and PUZ-F respectively, and it is associated with the very low amount
 371 of O₂ (respectively from 3*10⁻⁷ to 5*10⁻⁷ mol/l) these concentrations suggests that the water
 372 flows mainly through anoxic environment. Type I also highlights the occurrence of
 373 significant content in Ne, Ar and N₂ respectively up to 9*10⁻⁹, 2*10⁻⁵ and 7*10⁻⁴ mol/l, which
 374 are characteristic of the next cluster (Type II: N₂-rich springs) (Fig. 4).

375 4.2.1.2 Type II: N₂-rich springs

376 This second cluster concerns thermal springs (CALD, P-SOA, P-LAV, P-B),
 377 characterised by alkaline pH above 8.7 up to 9.7, very low mineralisation (mean value
 378 ≈330 μS/cm) and temperatures ranging from 30.4 to 54.7°C (Table 2) with Na and HCO₃⁻
 379 as dominant ions in all samples. This type is mainly represented by a high content in N₂
 380 between 4*10⁻⁴ and 6*10⁻⁴ mol/l associated with noble gas occurrence Ne (up to 8*10⁻⁹
 381 mol/l), Ar (up to 2*10⁻⁵ mol/l) and He (up to 8*10⁻⁷ mol/l) (Fig. 4).

382 4.2.1.3 Type III: CO₂-rich springs

383 The third cluster corresponds to the cold carbonated waters of Castagniccia and to two
 384 springs (FONT and ACQ) emerging in the sedimentary plain. These springs show
 385 temperatures ranging from 11°C (AMPU) to 22°C (ACQ), with a wide range of
 386 mineralisation from 230 μS/cm (S-SUP) to 2 890 μS/cm (ACQ) and up to 12 620 μS/cm
 387 (FONT) (Table 1). The Ca–HCO₃ water type is the dominant feature, even if a Na-Cl water
 388 type is observed at (FONT). This type presents a very high content in CO₂ with
 389 concentrations varying between 2*10⁻² and 4*10⁻² mol/l associated with N₂ occurrence up
 390 to 4*10⁻⁴ mol/l (Fig. 4).

391 4.2.2. Abundance classification

392 Three main gaseous provinces have been identified from the multi-criteria
 393 classification of gaseous discharge performed on the thermo-mineral groundwaters: CH₄
 394 and H₂S-rich (Type I), N₂-rich (Type II), and CO₂-rich (Type III). According to Faramawy
 395 *et al.* (2016), natural gas flux may have multiple origins and come from different processes
 396 such as, thermogenic processes forming CO₂, H₂S, H₂ and N₂, abiogenic processes forming
 397 CH₄ from mantle degassing or CO₂-reduction (Sherwood Lollar *et al.*, 2002; Rojey, 1997),
 398 but also from biogenic processes forming CH₄, CO₂ and H₂. In addition, two processes
 399 could also participate at the same time and provide the same gas content, as has already
 400 been observed in different regions (Štrbački *et al.*, 2020; Barros *et al.*, 2020; Moritz *et al.*,
 401 2015; Angelone *et al.*, 2005; Sherwood Lollar *et al.*, 2002).

402 As shown in Fig. 4, each type representing the major gas released is also associated
 403 with minor gases that are also released at the same time. The relative occurrence between

404 major and minor gas occurrence gives information about the processes involved, flow
405 patterns or combination processes occurring along flow paths. Indeed, the occurrence of
406 dissolved gases in groundwater is often the result of flow pattern mixing (Lee *et al.*, 2021;
407 Hiscock, 2009; Kipfer *et al.*, 2002). Influenced by physical degassing processes, these minor
408 gases appear in relative proportions as follows: N₂, Ar and Ne for Type I (CH₄ and H₂S-
409 rich), Ne and Ar with He for Type II (N₂-rich) and N₂ for Type III (CO₂-rich) (Fig. 4). This
410 observation highlights a minimal proportion of N₂ in each Type and the occurrence of Ar
411 and Ne in Type I and II. However, further study of the amount of dissolved gas is needed
412 to determine their origin.

413 4.2.3. Gas origin

414 To relate the composition of gases with their potential genesis processes, the 100*N₂-
415 CO₂-10000*Ar and the N₂-1 000*He-100*Ar ternary diagrams, proposed by Giggenbach *et al.*
416 (1983) and established from Powell and Cumming (2010), are shown in Fig. 5. This
417 figure displays groundwater dissolved gas content according to their relative content in
418 N₂, Ar, CO₂ (Fig. 5.A) and N₂, Ar, He (Fig 5.B).

419 In Figure 5.A, the trend towards the CO₂-vertex highlights the high amount of CO₂
420 contained in Type III springs and shows its seasonal degassing processes. The gas content
421 varies according to the month of sampling. This trend also shows that CO₂ content is not
422 linked to volcanic or to magmatic phenomena.

423 The literature highlights that the thermal decomposition of organic matter involves
424 alteration of the ¹³C-CH₄ isotopic signal varying from -60‰ to -20‰ (Faramawy *et al.*,
425 2016; Whiticar *et al.*, 1986; Berndt *et al.*, 1996). In contrast to abiogenic processes
426 responsible for the reduction of CO₂ into CH₄, mainly observed in hydrothermal water-
427 rock interactions and serpentinization of ultramafic rocks (Sherwood 2002), which shows
428 an enriched signal ¹³C-CH₄ > -60‰ (Agnew and Halihan, 2018; Faramawy *et al.*, 2016).
429 Biogenic processes due to biotic activity are responsible for gas production and show a
430 depleted ¹³C-CH₄ < -60‰ signature. In the regional literature, the δ¹³C-CH₄ signature was
431 performed on 3 carbo-gaseous springs of Castagniccia (Type III) and revealed an accurate
432 δ¹³C-CH₄ isotopic ratios of -26.1 (AMPU), -24.9 (PORT) and -21.6‰ (MOIT) (Berthier *et al.*,
433 1980). This signature is usually indicative of thermogenic processes corresponding to a
434 slow decomposition of organic material with depth because of an increase in pressure and
435 temperature on sedimentary rocks (Barros *et al.*, 2021, Faramawy *et al.*, 2016; Berndt *et al.*,
436 1996; Whiticar *et al.*, 1986). As observed in thermo-mineral waters from Italy by Minissale
437 (2004), a CO₂ content which comes from mantle degassing is added, along the
438 groundwater pathway, thermogenic- CO₂ coming from the remobilisation of
439 metamorphic decarbonation reactions of carbonated rocks (Barros *et al.*, 2021; Lavrushin
440 *et al.*, 2018; Petrović *et al.*, 2010; Thiébaud *et al.*, 2010). During the metamorphism of

441 sedimentary rocks, calcite reacts with SiO₂-rich fluids to produce wollastonite rock and
442 CO₂. The latter is then trapped by the schistosity of the rocks (Chiodini *et al.*, 2020). Some
443 wollastonite deposits were identified in Castagniccia and allow confirmation that the high
444 CO₂ content here is an addition of thermogenic CO₂ to mantle-degassing CO₂ (Vitale
445 Brovarone *et al.*, 2013; Malvoisin *et al.*, 2012; Ravna *et al.*, 2010).

446 The two figures (Fig 5.A and 5.B) highlight that all thermo-mineral groundwaters
447 encountered have an N₂/Ar ratio ranging between air and air-saturated water (ASW)
448 ratios. This ratio suggests that the N₂ component comes from trapped air, due to
449 atmospheric gases solubilised during rain infiltration (Fig. 5.B) (Epstein *et al.*, 2021, Powell
450 and Cumming, 2010; Minissale, 2004; Rojey, 1997; Giggenbach *et al.*, 1983). The relatively
451 higher content in Argon can be explained by radiogenic decay accumulating along flow
452 paths and translating long residence times, confirming previous isotopic dating results
453 (Dupuy *et al.*, 2021). Moreover, some studies also reveal that Ar could be also produced
454 by bacterial consumption of oxygen stock in an organic-rich environment. This process
455 added to water with a relatively shorter residence time could explain why the highest Ar-
456 content is observed during September, in PUZ-N and CAM-F springs, both emerging
457 from a rich organic matter environment (Faramawy *et al.*, 2016, Rojey *et al.*, 1997). As
458 observed on neighbouring Sardinia island, N₂-rich waters are aligned along the ASW -
459 Crust axis suggesting a general increase in crustal He produced by radioactive decay (Fig
460 5.B), mostly observable during the winter period (Amaral *et al.*, 2017; Minissale, 2004;
461 1999; Paternoster *et al.*, 2017). Helium is a radiogenic gas, produced from the radioactive
462 decay of U and Th present in weathered rocks from Earth's crust. Low in the atmosphere,
463 He is widely used as a tracker of volcanic activity, translating gases' deep origin from
464 mantle or crust degassing (Amaral *et al.*, 2017). Therefore, according to Hiscock (2009), its
465 accumulation in groundwater could also be due to long interaction time in U-Th- rich
466 rocks. N₂, associated with the He amount provides unequivocal evidence for a
467 contribution of deep non-atmospheric gas to these groundwater samples and a long
468 residence time (Casillas-Trasvina *et al.*, 2023, Zippa *et al.*, 2019, Kulongoski *et al.*, 2008).

469 4.3. Reactional processes

470 4.3.1. Processes identification

471 Principal component analysis (PCA) was performed from in-situ physical and chemical
472 parameters (T, pH, Eh, O₂, HCO₃), combined with gas abundance in April 2018, to confirm
473 the different processes occurring (Figure 6, Table 1). The first two components explain
474 50.35% of the total variance of the population. The component F1 is negatively correlated
475 with high CO₂ content, showing the CO₂ degassing (Type III), and positively correlated
476 with N₂, Ar and Ne characterising a crustal influence (Type I and Type II) (Mikhail and
477 Sverjensky, 2014). This last observation highlights the occurrence of deep influence also

478 on springs from the sedimentary plain (Type I). The component F2 is positively correlated
479 with O₂ content, highlighting mixing with surface waters concerning mainly one Type III
480 spring (AMPU). The component F3 is positively correlated with H₂S and CH₄-content and
481 negatively with He and Temperature; this axis differentiates biotic processes observed in
482 Type I from water with long residence times (Type II) (Dupuy *et al.*, 2021).

483 4.3.2. Biogenic gas evidence

484 The determination of recharge conditions allows the determination of the excess air (EA)
485 contribution. This value reflects the difference between groundwater gas concentration
486 observed in water and modelled concentration at the recharge area (Table 3). A positive
487 EA reflects a gas supply within the aquifer while a negative value means the involvement
488 of degassing processes, which can be also associated with dilution processes (mixing or
489 pressure variation due to the tectonic structure). EA determined on CO₂-free sources only,
490 Type I and Type II, shows values ranging between $-6.24 \cdot 10^{-3}$ (CAM-F) and $1.28 \cdot 10^{-3}$ (PUZ-
491 F). All springs show negative EA suggesting the involvement of dilution processes, except
492 for PUZ-F (Type II), which shows a positive value during the whole of the sampling
493 period. As suggested in the literature, the combination of CH₄ with a high amount of H₂S
494 in groundwater suggests the involvement of biotic processes (Tassi *et al.*, 2020 Lavrushin
495 *et al.*, 2018; Etiopie, 2017; Gilhooly *et al.*, 2014; Dupalová *et al.*, 2012; Machel *et al.*, 2001).
496 Associated with the ³⁴S-SO₄ and ³⁴S-H₂S data measured at the same mineral spring from
497 Dupuy *et al.* (2021), this positive EA value confirms that those biotic processes are
498 responsible for the increase of gas content in the aquifer, due to the biological degradation
499 of organic matter. This spring emerges from Miocene sediments known to contain thick
500 organic matter-rich marls (Aghione deposits of the Miocene). However, negative EA
501 values found on other Type I groundwaters (CAM-F & PUZ-N) also emerging from the
502 Miocene sediments are correlated with ³⁴S values measured in a previous study, which
503 does not show significant biotic activity (Dupuy *et al.*, 2021). The EA seems therefore to
504 be a good tracer of high biotic processes, showing equivalent results to ³⁴S analyses (Table
505 3).

506 4.3.3. Groundwater equilibration

507 Dissolved gas prevalence in groundwater is linked to physical and chemical
508 parameters and element equilibration state; a pH-Eh diagram was used to characterise
509 reservoir conditions affecting the gas content (Fig. 7, Table 2). Considering a stable pH
510 value, the variation of Eh ranging from -238 to 401 mV represents the water equilibrium
511 state and allows identifying equilibration with gas prevalence. All springs studied flow
512 mainly under confined reducing conditions (Fig. 7). The CO₂ and N₂-rich springs (Type II
513 and III) plot in the prevalence state of their predominant gas phases. Type I waters do not
514 plots either in the CH₄ or in the H₂S prevalence area, and highlight a higher Eh value than

515 expected for CH₄ and H₂S rich springs. Figure 7 shows that the CH₄ prevalence area is
516 close to the NH₄⁺ predominance area .

517 To identify springs influenced by abiotic processes, the simple NH₄⁺ occurrence in
518 groundwater was used as a witness of the water flowing through very reducing
519 conditions. Indeed, the NH₄⁺ is naturally released from the degradation of organic
520 nitrogen under highly reducing conditions. Its occurrence in groundwater, especially
521 when the physicochemical parameters of springs do not align with the NH₄⁺ prevalence
522 conditions, underscores water flowing through strong geologic confinement, as observed
523 for Type I and some springs of Type II. The NH₄⁺ values ranged from 0.01 (PUZ-N) to 2.17
524 mg/L (CAM-F) for Type I and ranged from 0.09 (MOIT) to 1.56 mg/L (FONT) for Type III.
525 The spring CAM-F displays the highest concentration in NH₄⁺.

526 The fact that very reducing conditions are reached may cause a secondary production
527 of CH₄ from CO₂, by processes referred to here as abiotic, and explain the high CH₄, CO₂
528 and H₂S gas content measured in some groundwaters (Fig. 8) (Tassi *et al.*, 2020; Marques
529 *et al.*, 2018; Minissale *et al.*, 2000; Paull *et al.*, 2000). Indeed, results from Figure 7 associated
530 with the binary diagrams (Fig. 8), allow to distinguish the gas variation involved by the
531 biotic activity from abiotic production with the example of the CAM-F springs
532 (Chelnokov *et al.*, 2018; Jenden *et al.*, 2015). Then, the re-equilibration of water during the
533 up-flow under oxidative conditions explains the Eh value observed at the discharge.

534 4.4. Flowpath

535 4.4.1 From degassing to local flow information

536 As suggested by the high dissolved gas content and confirmed by the negative EA
537 (Table 3), degassing processes are important in these thermo-mineral groundwaters. The
538 degassing process can result from factors such as dilution, mixing, or the local tectonic
539 structure. This latter can lead to variations in pressure, which, in turn, influence the
540 release of gases depending on the solubility conditions of each gas. To discriminate
541 dilution at one side, with modern water at another side, from mixing between two
542 different aquifer units during upwelling, anthropogenic gas (CFC and SF₆) analyses were
543 initially performed (Table 4). Results show that SF₆ values ranged from 0.89 (P-B) to 8.33
544 (FONT) pptv, 19 (PUZ-F) to 166.82 (S-SOT) pptv for CFC-12, from 88.03 (FORC) to 283.04
545 pptv (P-B) for CFC-11 and from 3.78(P-LAV) to 18.27 pptv (PUZ-F) for CFC-113 (Table 4).
546 These values show a low of SF₆, CFC-12 and CFC-113 with an uncorrelated high amount
547 of CFC-11. To explain this, it is acquired that if atmospheric contamination occurs all CFCs
548 gases should be impacted in the same proportions (Cartwright *et al.*, 2017; Darling *et*
549 *al.*, 2012). So only a few natural processes could explain the relative amount of variation
550 between CFCs as microbial breakdown or sorption, but neither of these can explain the

551 proportion obtained here, from springs in different geological contexts (Chambers *et al.*,
552 2019; Kotowski *et al.*, 2019). Moreover, according to Beyerle *et al.* (1999), these
553 anthropogenic gases are responsive to Excess Air formation and degassing processes.
554 Degassing processes could then explain the relative proportions observed which are
555 inversely proportional to their AE sensitivity (Cartwright *et al.*, 2017). Even if degassing
556 processes influence the anthropogenic gas content in groundwater, their occurrence in
557 groundwater highlights a dilution process with modern water and should be confirmed
558 by the ^3H content (Table 3).

559 Tritium measured in groundwater ranges from 0 (P-X) to 2.3 TU (PARD); knowing that
560 the average ^3H content in Corsican rainwater is about 8 TU (Juhlke *et al.*, 2020) it can be
561 concluded that Type I are old water diluted by modern surface waters or shallow
562 groundwaters (characterised by the presence of anthropogenic gases, negative EA and
563 with noticeable ^3H amount). By comparison, the negative AE combined with groundwater
564 deprived of ^3H characterises Type II as composed of old groundwater only. Type III
565 groundwater shows the widest diversity of flow path contributions. In this category (CO_2 -
566 rich springs) some springs are mainly composed of old water while many other springs
567 result from mixing processes between old water diluted with an actual water fraction
568 (Table 3) containing anthropogenic gases and ^3H .

569 4.4.2 Influence of regional flow

570 Noble gases found in groundwater reveal the recharge conditions history. It is usually
571 admitted that the higher the concentration of noble gases in the water, the colder is the
572 recharge temperatures observed (Hiscock, 2009; Kipfer *et al.*, 2002). The Ar and N_2
573 concentrations are displayed in Fig. 9. Carbogaseous waters (Type III) show the lowest
574 amount of noble gas, due to their intensive degassing. Fig. 9 highlights the CH_4 -rich
575 waters (Type I) springing out from the sedimentary plain and show a higher or equivalent
576 amount of noble gas than thermal springs (Type II). However, this observation is different
577 from the recharge altitude estimation calculated from $\delta^2\text{H}$ and $\delta^{18}\text{O}$ data measured in this
578 study (Table 2). These values show a differentiated recharge altitude ranging from 764 to
579 900 m asl for Type II and from 78 to 290 m asl for Type I. The noble gas concentration
580 suggests that, even if most groundwater flow in the sedimentary plain comes from a local
581 recharge, some springs from the plain (Type I) can also be supplied by a deeper up-flow
582 coming from a higher altitude.

583 As detailed by Elena *et al.* (2020), helium is a highly volatile radiogenic gas, its
584 accumulation in groundwater is usually proportional to the increasing depth or residence
585 time at the contact with source-rocks (Werner *et al.*, 2022; Casillas-Trasvina *et al.*, 2022;
586 Karolyt  *et al.*, 2019; Kulongoski *et al.*, 2008). The measure of He excess is therefore
587 significant (analytical threshold $\approx 10^{-9}$ cm³STP/g) due to accumulation along the flow line

588 and indicates very long circulatory processes. All (non-carbogaseous) springs show an
589 excess of He. The greatest excess (from 10^{-5} and 10^{-6} cm³STP/g) is observed for Type III,
590 however, the amount of He excess in the sedimentary plain springs (Type I) confirms their
591 supply by the deep flow, having a long residence time.

592 **4.4.3 Conceptual model of groundwater flow towards thermo-mineral springs**

593 From the geochemical, the water stable isotopic and gases dataset obtained a
594 conceptual hydrogeological model of the region is proposed (Fig. 10). It shows that
595 meteoric water infiltrated at high altitudes (>800 m asl) infiltrates into granitic rocks
596 through major faults and deep fractures. Water is then warmed by the natural geothermal
597 gradient until the shallower part of the crust where water is enriched with high amounts
598 of N₂, He, and low amounts of CO₂. The local geostructure allows the release of dissolved
599 gases up to the near surface (Type II). However, this study reveals that the type II (N₂-
600 rich) also supplies through depth all other thermal and mineral springs emerging in the
601 sedimentary plain (Fig. 11). Depending on waters and rocks encountered along the
602 gaseous up-flow, this regional gaseous signature is locally modified by abiotic and biotic
603 processes. During the flow path through metamorphic rocks, the deep gaseous flux is
604 mixed with carbonated waters coming from a local recharge. The water circulation
605 through these rocks allows the mobilisation of thermogenic CO₂ coming from
606 metamorphosed schists (Type III). This high amount of CO₂ increases the degassing
607 process of low soluble gases as noble gas originating from the regional gaseous flux.

608 Carbogaseous water also springs out in the southern part of the sedimentary plain, at
609 the interface of the different geological units, where the metamorphosed rocks are
610 overlapped by an impermeable geological layer of Eocene flyschs. Here also
611 metamorphosed rocks supply the sedimentary plain at depth with N₂ and CO₂ gases
612 which are subsequently influenced along their pathway through deep anoxic and very
613 reducing conditions. This abiotic process is responsible for the N₂ reduction into NH₄⁺ and
614 CO₂ into CH₄ increasing NH₄⁺ and CH₄ content in groundwater (Fig. 11). Then, still
615 supplied by a local recharge, the water flows in contact with the organic material
616 contained in the Miocene sediments. Biotic processes alter the sulfate isotopic and
617 geochemical composition of those waters and increase the H₂S amount in surface waters
618 (Type I) (Fig. 10 and 11).

619 Using this innovative and complex combination of tools, investigations highlight the
620 occurrence of a regional gas supply observed in all thermo-mineral waters of the eastern part
621 of Corsica Island, even in a non-tectonically active zone. The geological structural complexity
622 of the island is responsible for a wide variety of processes affecting gas and water composition
623 and explains the high diversity of thermo-mineral water observed, as shown in Fig. 10. The
624 complexity and the diversity of processes accumulating along the regional path confirm the

625 involvement of gas and water mixing processes between the different geological units. To
626 achieve a more sustainable use of thermo-mineral springs on the island of Corsica,
627 quantifying the interplay between regional and local flows must be considered for future
628 research. Indeed, due to the complexity of the flow paths involving, deep upwelling,
629 interactions with the local geological matrix and mixing with phreatic waters, quantification
630 of mixing ratios will be helpful in a further attempt to contribute to a more sustainable
631 exploitation of the island's thermo-mineral springs.

632 5. Conclusion

633 These investigations aimed to provide new information on the accumulation of
634 hydrogeological processes along groundwater flow-paths within tectonically non-active
635 zones. Our findings demonstrate that groundwater gas contents can provide an almost
636 complete assessment of hydrogeological processes (abiotic and biotic) occurring on both
637 regional and local scales. This approach reveals not easily discernible insights by using
638 more conventional hydrogeochemical and isotopic tools.

639 The use of dissolved gases as tracers circumvents the methodological constraints
640 often encountered with classic tools, due to the presence of CO₂, iron, or sulfur, which can
641 constrain the water analyses. This unconventional method enables us to identify the flow
642 paths irrespective of water type or encountered geological units making analysis possible
643 independently of water intrinsic properties (conductivity, pH, carbon or sulfide content).

644 In conclusion, studying dissolved gas content is an unconventional yet valuable tool,
645 providing qualitative information about aquifer hydrogeological functioning such as the
646 recharge conditions, the regional flow paths, hydrogeological compartments mixing
647 (deep versus phreatic) and the impact of bacterial activity on water composition.

648 However, it is important to acknowledge several limitations, which can be
649 categorised into two: practical and technical aspects, as well as more generalised data
650 interpretation. Practical and technical limitations include the need for careful sampling,
651 rapid gas sample analysis (< 48H) and cautious transportation (avoiding sudden pressure
652 changes). To respectively avoid, atmospheric contamination, gas consumption or
653 production by biotic activity, or artificial degassing which could introduce results bias,
654 especially for carbonaceous samples. The limitations of the methodology and data
655 interpretation arise from the high diversity of dissolved gases measured in this study.
656 Resulting in contrasting gas signatures that are easy to identify and differ significantly
657 from the uncertainties associated with our analytical tools. Further studies are needed to
658 evaluate the applicability and effectiveness of this methodology when applied to springs
659 with lower geochemical and gas diversity.

660 To pave the way for further research, it remains to be seen whether the dissolved gas
661 content can be used to mathematically quantify groundwater mixing along the flow
662 path. Quantifying flow paths at the origin of mineral water genesis is imperative for the
663 effective protection and management of exploited spa or bottled springs. Understanding
664 processes involved in gases and water release is essential to ensure the sustainability and
665 quality of these valuable resources. It would allow the identification of potential sources
666 of contamination, monitor the influence of biotic factors, and assess the impact of external
667 forces, such as climate change and anthropogenic activities. By quantifying flow paths,
668 we gain insights into the hydrogeological dynamics that shape mineral water
669 composition, enabling us to make informed decisions for resource preservation. This
670 knowledge empowers stakeholders to safeguard the integrity of spa and bottled springs,
671 ensuring their long-term availability and benefit to society. This significance is heightened
672 when considering that currently remote regions in Europe, such as those hosting
673 UNESCO World Heritage sites, have their economies dependent solely on the spa tourism
674 and social appeal of these historically renowned mineral springs since the 18th century.

675 **DECLARATION OF COMPETING INTEREST**

676 The authors declare that they have no known competing financial interests or personal
677 relationships that could have appeared to influence the work reported in this paper.

678 **ACKNOWLEDGEMENT**

679 This research was supported by the *Culletivittà di Corsica* through the GERHYCO
680 interdisciplinary project dedicated to water management, ecology and hydro-ecosystem
681 services in an island context.

682 **DATA AVAILABILITY**

683 Data will be made available on request.

684

685 List of Figures

686 Figure 1 : Ombrothermal diagrams displaying low-land and in-land mean climatic conditions at 3 stations
 687 of the study area (Bastia and Solenzara for the low-land and Corte for the in-land climatic
 688 conditions). Data is collected by the French weather forecast office and it' is available online. Data
 689 displayed here is compiled from 1950 to 2020. This diagram displays the total monthly
 690 precipitation in mm and the monthly minimum., maximum. and mean temperatures express in
 691 degree centigrade and gives relative expression of summer drought. The intensity and duration
 692 of the dry season based on the intersections of the Temperature curves and the Precipitation one.

693 Figure 2: Location and simplified geology of the studied area. Location and typology of the thermo-mineral
 694 springs. The spring symbols describe gas type; spring name colour refers to the geochemical water
 695 type.

696 Figure 3: Piper diagram of Eastern Corsica thermo-mineral water samples (N=259). Circle around spring
 697 symbols represents quantitative information on the total dissolved solids (T.D.S.) in
 698 groundwaters. For more accurate representation, the TDS values are proportionally magnified by
 699 5.

700 Figure 4: Multi-criteria classification and characterisation of thermal and mineral water samples were
 701 carried out applying hierarchical type analysis (HCA) on gas chemical composition obtained in
 702 April on 9 springs. This heatmap is a graphic representation of data where gas abundances (Ne,
 703 He, Ar, N₂, H₂, CO₂, O₂, CH₄, H₂S) are depicted by colour, from low concentration (dark blue) to
 704 high concentration (deep red).

705 Figure 5: Ternary diagrams displaying dissolved gas content in thermo-mineral waters after Giggenbach *et*
 706 *al.* (1983). All springs are displayed by code name then by the number of the sampling month. The
 707 ternary diagram (A) displays N₂-CO₂-Ar to illustrate the relative CO₂ contribution of magmatic,
 708 meteoric and volcanic sources of gases in Corsican thermo-mineral springs. The meteoric
 709 component is limited by the air ratio (N₂/Ar=84) and the air saturated water (ASW) ratio
 710 (N₂/Ar=38), the volcanic component by (CO₂/N₂=200), and it confirms the predominantly meteoric
 711 origin of these compounds. The lines between CO₂ apex, ASW and Air points indicate the effect
 712 of shallow contamination on dissolved gases. The ternary diagram (B) displays N₂-He-Ar to
 713 illustrate the relative contribution from magmatic, meteoric or crustal sources of gases in thermo-
 714 mineral springs. The meteoric component is limited by the air ratio (N₂/Ar=84) and the air
 715 saturated water (ASW) ratio (N₂/Ar=38) and it confirms the predominantly meteoric origin of
 716 these compounds. (*) Sampling air contamination.

717 Figure 6: Principal Component Analysis (PCA) discriminating processes and flows involved in spring water
 718 composition.

719 Figure 7: Pourbaix diagram explaining the predominance of CO₂, N₂ and CH₄ gases. Eh vs. pH values of
 720 thermomineral springs were plotted to determinate waters influenced by reductive conditions.

721 Figure 8: Binary diagram of CH₄, H₂S and CO₂ abundances observed in waters. Biogenic influence is evidenced
 722 with the line 1:1 due to bacterial activity (Chelnokov *et al.*, 2018)

723 Figure 9: Binary diagram of N₂ and Ar in mol/L in thermo-mineral waters. Regression lines are displayed

- 724 by colour according to each type: CO₂, N₂ or CH₄ rich water.
- 725 Figure 10. Hydrogeological conceptual model of thermo-mineral waters from the eastern part of Corsica.
726 Established from gas composition in order to discriminate flow and processes involved along the
727 regional continuous flow path from mountains to plain.
- 728 Figure 11. Major gas-related processes according to each spring type. Type I : CH₄ & H₂S rich, Type II : N₂
729 rich and Type III : CO₂ rich. Oxi. Proc. : Oxidation process ; Red. Proc. : Reduction process.
- 730 List of tables
- 731 Table 1: Information about sites, spring localities, code name, type and altitude.
- 732 Table 2: Field parameters, hydrochemical and isotopic contents of thermo-mineral groundwaters.
- 733 Table 3: Concentration of dissolved gas sampled with analytical error. Helium and excess air calculation results.
734 (<LOD) limit of detection, (n.m) non-measured, (-) calculation not realisable due to high CO₂ degassing.
- 735 Table 4: CFC and SF₆ concentrations measured in water in pmol/L and pptv
- 736

737 REFERENCES

- 738 Aeschbach-Hertig, W., Peeters, F., Beyerle, U., Kipfer, R., 1999. Interpretation of dissolved atmospheric noble gases in
739 natural waters. *Water Resources Research* 35, 2779–2792. <https://doi.org/10.1029/1999WR900130>.
- 740 Agnew, R.J., Halihan, T., 2018. Why Springs Bubble: A Framework for Gas Discharge in Groundwater. *Groundwater*
741 56: 859-870. <https://doi.org/10.1111/gwat.12789>.
- 742 Amaral, H.I.F., Midões, C., Kipfer, R., 2017. Helium evidences for mantle degassing in the groundwater of Madeira
743 Island – Portugal. *Applied Geochemistry* 81, 98–108. <https://doi.org/10.1016/j.apgeochem.2017.03.019>.
- 744 Amaudric, D.C.S., 1973. Les relations entre Schistes lustres et Flyschs autochtones dans le Sud de la Corse alpine.
745 *Geologie Alpine* 49, 5–12.
- 746 Angelone, M., Gasparini, C., Guerra, M., Lombardi, S., Pizzino, L., Quattrocchi, F., Sacchi, E., Zuppi, G.M., 2005. Fluid
747 geochemistry of the Sardinian Rift-Campidano Graben (Sardinia, Italy): fault segmentation, seismic quiescence of
748 geochemically “active” faults, and new constraints for selection of CO₂ storage sites. *Applied Geochemistry* 20, 317–
749 340. <https://doi.org/10.1016/j.apgeochem.2004.08.008>.
- 750 Aquilina, L., and J.-R. De Dreuzy. 2011. ‘Relationship of Present Saline Fluid with Paleomigration of Basinal Brines at
751 the Basement/Sediment Interface (Southeast Basin – France)’. *Applied Geochemistry* 26 (12): 1933–45.
752 <https://doi.org/10.1016/j.apgeochem.2011.06.022>.
- 753 Barros, R., Defourny, A., Collignon, A., Jobe, P., Dassargues, A., Piessens, K., Welkenhuysen, K., 2020. A review of the
754 geology and origin of CO₂ in mineral water springs in east Belgium. *Geol. Belg.* <https://doi.org/10.20341/gb.2020.023>.
- 755 Benavente, O., Tassi, F., Reich, M., Aguilera, F., Capecchiacci, F., Gutiérrez, F., Vaselli, O., Rizzo, A., 2016. Chemical and
756 isotopic features of cold and thermal fluids discharged in the Southern Volcanic Zone between 32.5°S and 36°S:
757 Insights into the physical and chemical processes controlling fluid geochemistry in geothermal systems of Central
758 Chile. *Chemical Geology* 420, 97–113. <https://doi.org/10.1016/j.chemgeo.2015.11.010>.
- 759 Berndt, M.E., Allen, D.E., Seyfried Jr, W.E., 1996. Reduction of CO₂ during serpentinization of olivine at 300 C and 500
760 bar. *Geology* 24, 351–354.
- 761 Berthier, F., Demange, J., Desplan, A., 1980. Etude préliminaire des ressources géothermiques de la Corse (Rapport final
762 No. 80SGN784GTH). BRGM.
- 763 Beyerle, U., Aeschbach-Hertig, W., Hofer, M., Imboden, D.M., Baur, H., Kipfer, R., 1999. Infiltration of river water to a
764 shallow aquifer investigated with 3H/3He, noble gases and CFCs. *Journal of Hydrology* 220, 169–185.
- 765 Bräuer, K., Kämpf, H., Niedermann, S., Wetzell, H.-U., 2017. Regional distribution pattern of carbon and helium isotopes
766 from different volcanic fields in the French Massif Central: Evidence for active mantle degassing and water
767 transport. *Chemical Geology, Progress in the Application of Gas Geochemistry to Geothermal, Tectonic and*
768 *Magmatic Studies* 469, 4–18. <https://doi.org/10.1016/j.chemgeo.2017.04.004>.
- 769 Bruno, C., Dupré, G., Giorgetti, G., Giorgetti, J.P., Alesandri, J., 2001. Chi tempu face?: météorologie, climat et
770 microclimats de la Corse., CRDP de Corse.
- 771 Busenberg, E., Plummer, L.N., 1992. Use of chlorofluorocarbons (CCl₃F and CCl₂F₂) as hydrologic tracers and age-
772 dating tools: The alluvium and terrace system of central Oklahoma. *Water Resources Research* 28, 2257–2283.
773 <https://doi.org/10.1029/92WR01263>.
- 774 Caballero, Y., Lachassagne, P., Ladouche, B., 2006. Contribution à l'évaluation de la ressource en eau des aquifères de

- 775 socle des roches granitiques de Corse (Rapport final No. BRGM/RP-54541-FR).
- 776 Caritg, S., 2009a. Carte géologique harmonisée du département de la Corse du sud : Notice explicative (Rapport final
777 No. brgm/rp-57749-FR). BRGM.
- 778 Caritg, S., 2009b. Carte géologique harmonisée du département de la haute-Corse : Notice explicative (Rapport final
779 No. BRGM/RP-57748-FR). BRGM.
- 780 Cartwright, Ian, D. Cendón, M. Currell, and K. Meredith. 2017. 'A Review of Radioactive Isotopes and Other Residence
781 Time Tracers in Understanding Groundwater Recharge: Possibilities, Challenges, and Limitations'. *Journal of*
782 *Hydrology* 555 (December): 797–811. <https://doi.org/10.1016/j.jhydrol.2017.10.053>.
- 783 Casillas-Trasvina, A., B. Rogiers, K. Beerten, J. Pärn, L. Wouters, and K. Walraevens. 2022. 'Using Helium-4, Tritium,
784 Carbon-14 and Other Hydrogeochemical Evidence to Evaluate the Groundwater Age Distribution: The Case of the
785 Neogene Aquifer, Belgium'. *Journal of Hydrology X* 17:100132. <https://doi.org/10.1016/j.hydroa.2022.100132>.
- 786 Chambers, L.A., Goody, D.C., Binley, A.M., 2019. Use and application of CFC-11, CFC-12, CFC-113 and SF6 as
787 environmental tracers of groundwater residence time: A review. *Geoscience Frontiers* 10, 1643–1652.
- 788 Chatton, E., Labasque, T., de La Bernardie, J., Guihéneuf, N., Bour, O., Aquilina, L., 2017. Field Continuous
789 Measurement of Dissolved Gases with a CF-MIMS: Applications to the Physics and Biogeochemistry of
790 Groundwater Flow. *Environ. Sci. Technol.* 51, 846–854. <https://doi.org/10.1021/acs.est.6b03706>.
- 791 Chelnokov, G.A., Bragin, I.V., Kharitonova, N.A., 2018. Geochemistry of mineral waters and associated gases of the
792 Sakhalin Island (Far East of Russia). *Journal of Hydrology* 559, 942–953. <https://doi.org/10.1016/j.jhydrol.2018.02.049>.
- 793 Chiodini, G., Cardellini, C., Caliro, S., Avino, R., Donnini, M., Granieri, D., Morgantini, N., Sorrenti, D., Frondini, F.,
794 2020. The hydrothermal system of Bagni San Filippo (Italy): fluids circulation and CO₂ degassing. *Italian Journal of*
795 *Geosciences* 139, 383–397. <https://doi.org/10.3301/IJG.2020.12>.
- 796 Craw, D., Upton, P., Horton, T., Williams, J., 2013. Migration of hydrothermal systems in an evolving collisional orogen,
797 New Zealand. *Miner Deposita* 48, 233–248. <https://doi.org/10.1007/s00126-012-0421-8>.
- 798 D'Amore, F., Fancelli, R., Caboi, R., 1987. Observations on the application of chemical geothermometers to some
799 hydrothermal systems in Sardinia. *Geothermics* 16, 271–282. [https://doi.org/10.1016/0375-6505\(87\)90006-X](https://doi.org/10.1016/0375-6505(87)90006-X).
- 800 Darling, W. G., D. C. Goody, A. M. MacDonald, and B. L. Morris. 2012. 'The Practicalities of Using CFCs and SF6 for
801 Groundwater Dating and Tracing'. *Applied Geochemistry*, 13th International Symposium on Water-Rock
802 Interaction (WRI -13), 27 (9): 1688–97. <https://doi.org/10.1016/j.apgeochem.2012.02.005>.
- 803 Dewandel, B., Lachassagne, P., Zaidi, F.K., Chandra, S., 2011. A conceptual hydrodynamic model of a geological
804 discontinuity in hard rock aquifers: Example of a quartz reef in granitic terrain in South India. *Journal of Hydrology*
805 405, 474–487. <https://doi.org/10.1016/j.jhydrol.2011.05.050>.
- 806 Di Rosa, M., De Giorgi, A., Marroni, M., Vidal, O., 2017. Syn-convergence exhumation of continental crust: evidence
807 from structural and metamorphic analysis of the Monte Cecu area, Alpine Corsica (Northern Corsica, France).
808 *Geological Journal* 52, 919–937. <https://doi.org/10.1002/gj.2857>
- 809 Dominici, R., Iundt, F., Juncy, G., Mickaelly, B., 1986. Prospection des anomalies gazeuses liées a l'hydrothermalisme
810 de Puzichellu - commune d'Aghione (Haute Corse) (No. 86SGN002CSC), BRGM. Bastia.
- 811 Dupalová, T., Sracek, O., Vencelides, Z., Žák, K., 2012. The origin of thermal waters in the northeastern part of the Eger
812 Rift, Czech Republic. *Applied geochemistry* 27, 689–702.

- 813 Dupuy, M., Garel, E., Huneau, F., Santoni, S., Di Rosa, M., Mattei, A., 2021. Geochemical and isotope characterisation
814 of thermo-mineral springs of Corsica Island: from geological complexity to groundwater singularity. *Water* 13, 2413.
815 <https://doi.org/10.3390/w13172413>.
- 816 Elena, F., Vasiliy, L., Natalia, K., Arslan, S., Elena, M., Ekaterina, B., Anna, K., Alexey, M., Elena, B., 2020. Hydrogeology
817 and hydrogeochemistry of mineral sparkling groundwater within Essentuki area (Caucasian mineral water region).
818 *Environmental Earth Sciences* 79, 1–12.
- 819 Epstein, Gabe S., Gray E. Bebout, B.W. Christenson, H. Sumino, I. Wada, C. Werner, and D.R. Hilton. 2021. 'Cycling of
820 CO₂ and N₂ Along the Hikurangi Subduction Margin, New Zealand: An Integrated Geological, Theoretical, and
821 Isotopic Approach'. *Geochemistry, Geophysics, Geosystems* 22 (9): e2021GC009650.
822 <https://doi.org/10.1029/2021GC009650>.
- 823 Etiopie, G., 2017. Abiotic Methane in Continental Serpentinization Sites: An Overview. *Procedia Earth and Planetary
824 Science, 15th Water-Rock Interaction International Symposium, WRI-15 17, 9–12.*
825 <https://doi.org/10.1016/j.proeps.2016.12.006>.
- 826 Everitt, B.S., Dunn, G., 2001. Principal Components Analysis, in: *Applied Multivariate Data Analysis*. John Wiley &
827 Sons, Ltd, pp. 48–73. <https://doi.org/10.1002/9781118887486.ch3>
- 828 Faramawy, S., Zaki, T., Sakr, A.A.-E., 2016. Natural gas origin, composition, and processing: A review. *Journal of
829 Natural Gas Science and Engineering* 34, 34–54. <https://doi.org/10.1016/j.jngse.2016.06.030>
- 830 Genevier, M., Mardhel, V., Frissant, N., 2011. Actualisation de la synthèse hydrogéologique de la région Corse (Rapport
831 final No. BRGM/RP-59924-FR). BRGM.
- 832 Giggenbach, W.F., 1991. Chemical techniques in geothermal exploration. Application of geochemistry in geothermal
833 reservoir development 119–144.
- 834 Giggenbach, W.F., 1988. Geothermal solute equilibria. Derivation of Na-K-Mg-Ca geoindicators. *Geochimica et
835 Cosmochimica Acta* 52, 2749–2765. [https://doi.org/10.1016/0016-7037\(88\)90143-3](https://doi.org/10.1016/0016-7037(88)90143-3).
- 836 Giggenbach, W.F., Gonfiantini, R., Jangi, B.L., Truesdell, A.H., 1983. Isotopic and chemical composition of parbati valley
837 geothermal discharges, North-West Himalaya, India. *Geothermics* 12, 199–222. [https://doi.org/10.1016/0375-6505\(83\)90030-5](https://doi.org/10.1016/0375-6505(83)90030-5).
- 839 Gilhooly, W.P., Fike, D.A., Druschel, G.K., Kafantaris, F.-C.A., Price, R.E., Amend, J.P., 2014. Sulfur and oxygen isotope
840 insights into sulfur cycling in shallow-sea hydrothermal vents, Milos, Greece. *Geochem Trans* 15, 12.
841 <https://doi.org/10.1186/s12932-014-0012-y>.
- 842 Goswami, S., AK. Rai, and S. Tripathy. 2022. 'Re-Visiting Geothermal Fluid Circulation, Reservoir Depth and
843 Temperature of Geothermal Springs of India'. *Journal of Hydrology* 612 (September): 128131.
844 <https://doi.org/10.1016/j.jhydrol.2022.128131>.
- 845 Grasby, S.E., Hutcheon, I., Krouse, H.R., 2000. The influence of water-rock interaction on the chemistry of thermal
846 springs in western Canada. *Applied Geochemistry* 15, 439–454. [https://doi.org/10.1016/S0883-2927\(99\)00066-9](https://doi.org/10.1016/S0883-2927(99)00066-9).
- 847 Gueydan, F., Brun, J.-P., Phillippon, M., Noury, M., 2017. Sequential extension as a record of Corsica Rotation during
848 Apennines slab roll-back. *Tectonophysics, Evolution of fore-arc and back-arc sedimentary basins with focus on the
849 Japan subduction system and its analogues* 710–711, 149–161. <https://doi.org/10.1016/j.tecto.2016.12.028>.
- 850 Hiscock, K.M., 2009. *Hydrogeology: principles and practice*. John Wiley & Sons.

- 851 Jenden, P.D., Titley, P.A., Worden, R.H., 2015. Enrichment of nitrogen and ^{13}C of methane in natural gases from the
852 Khuff Formation, Saudi Arabia, caused by thermochemical sulfate reduction. *Organic Geochemistry* 82, 54–68.
- 853 Juhlke, T.R., Sültenfuß, J., Trachte, K., Huneau, F., Garel, E., Santoni, S., Barth, J.A., Geldern, R. van, 2020. Tritium as a
854 hydrological tracer in Mediterranean precipitation events. *Atmospheric Chemistry and Physics* 20, 3555–3568.
- 855 Karolytè, R., Johnson, G., Györe, D., Serno, S., Flude, S., Stuart, F.M., Chivas, A.R., Boyce, A., Gilfillan, S.M.V., 2019.
856 Tracing the migration of mantle in gas fields and mineral water springs in south-east Australia using noble gas and
857 stable isotopes. *Geochimica et Cosmochimica Acta* 259, 109–128. <https://doi.org/10.1016/j.gca.2019.06.002>.
- 858 Karolytè, R., Serno, S., Johnson, G., Gilfillan, S.M.V., 2017. The influence of oxygen isotope exchange between CO_2 and
859 H_2O in natural CO_2 -rich spring waters: Implications for geothermometry. *Applied Geochemistry* 84, 173–186.
860 <https://doi.org/10.1016/j.apgeochem.2017.06.012>.
- 861 Kim, K.-H., Yun, S.-T., Yu, S., Choi, B.-Y., Kim, M.-J., Lee, K.-J., 2020. Geochemical pattern recognitions of deep thermal
862 groundwater in South Korea using self-organizing map: Identified pathways of geochemical reaction and mixing.
863 *Journal of Hydrology* 589, 125202. <https://doi.org/10.1016/j.jhydrol.2020.125202>
- 864 Kipfer, R., Aeschbach-Hertig, W., Peeters, F., Stute, M., 2002. Noble gases in lakes and ground waters. *Reviews in*
865 *mineralogy and geochemistry* 47, 615–700.
- 866 Kotowski, T., L. Chudzik, and J. Najman. 2019. ‘Application of Dissolved Gases Concentration Measurements,
867 Hydrochemical and Isotopic Data to Determine the Circulation Conditions and Age of Groundwater in the Central
868 Sudetes Mts’. *Journal of Hydrology* 569 (February): 735–52. <https://doi.org/10.1016/j.jhydrol.2018.12.013>.
- 869 Kulongoski, Justin T., David R. Hilton, Richard G. Cresswell, Stephen Hostetler, and Gerry Jacobson. 2008. ‘Helium-4
870 Characteristics of Groundwaters from Central Australia: Comparative Chronology with Chlorine-36 and Carbon-
871 14 Dating Techniques’. *Journal of Hydrology* 348 (1): 176–94. <https://doi.org/10.1016/j.jhydrol.2007.09.048>.
- 872 Lachassagne, P., 2011. The fracture permeability of Hard Rock Aquifers is due neither to tectonics, nor to unloading,
873 but to weathering processes. *Terra Nova* 145–161. <https://doi.org/10.1111/j.1365-3121.2011.00998.x>.
- 874 Lavrushin, V.Y., Israfilov, Y.G., Polyak, B.G., Pokrovsky, B.G., Bujakaite, M.I., Kamensky, I.L., 2018. Conditions of the
875 formation of thermomineral waters in the Talysh fold zone of the Lesser Caucasus (Azerbaijan) based on isotope-
876 geochemical data ($^3\text{He}/^4\text{He}$, $\delta^{13}\text{C}_{\text{CO}_2}$, $\delta^{13}\text{C}_{\text{CH}_4}$, $\delta^{15}\text{N}-\text{N}_2$, $^{87}\text{Sr}/^{86}\text{Sr}$, $\delta\text{D}-\text{H}_2\text{O}$, and $\delta^{18}\text{O}-\text{H}_2\text{O}$). *Lithology and*
877 *Mineral Resources* 53, 53–75. <https://doi.org/10.1134/S0024490217060050>.
- 878 Lee, J.M., Koh, D.-C., Chae, G.-T., Kee, W.-S., Ko, K.-S., 2021. Integrated assessment of major element geochemistry and
879 geological setting of traditional natural mineral water sources in South Korea at the national scale. *Journal of*
880 *Hydrology* 598, 126249. <https://doi.org/10.1016/j.jhydrol.2021.126249>.
- 881 Loÿe-Pilot, M.-D., Durand-Delga, M., Feinberg, H., Gourinard, Y., Magné, J., 2004. Les formations burdigaliennes de
882 Corse orientale dans leur cadre géodynamique. *Comptes Rendus Geoscience* 336, 919–930.
883 <https://doi.org/10.1016/j.crte.2004.02.011>.
- 884 Machel, H.G., 2001. Bacterial and thermochemical sulfate reduction in diagenetic settings: Old and new insights.
885 *Sedimentary Geology* 33.
- 886 Malvoisin, B., Chopin, C., Brunet, F., Galvez, M.E., 2012. Low-temperature Wollastonite Formed by Carbonate
887 Reduction: a Marker of Serpentinite Redox Conditions. *Journal of Petrology* 53, 159–176.
888 <https://doi.org/10.1093/petrology/egr060>.
- 889 Marques, J.M., Eggenkamp, H.G.M., Carreira, P.M., Antunes da Silva, M., 2020. Origin and evolution of Cl in CO_2 -rich

- 890 thermal and mineral waters from northern Portugal. *Applied Geochemistry* 116, 104569.
891 <https://doi.org/10.1016/j.apgeochem.2020.104569>.
- 892 Marques, J.M., Etiopie, G., Neves, M.O., Carreira, P.M., Rocha, C., Vance, S.D., Christensen, L., Miller, A.Z., Suzuki, S.,
893 2018. Linking serpentinization, hyperalkaline mineral waters and abiotic methane production in continental
894 peridotites: an integrated hydrogeological-bio-geochemical model from the Cabeço de Vide CH₄-rich aquifer
895 (Portugal). *Applied Geochemistry* 96, 287–301. <https://doi.org/10.1016/j.apgeochem.2018.07.011>.
- 896 Marques, J.M., Carreira, P.M.M., Aires-Barros, L., Graça, R.C., 2000. Nature and role of CO₂ in some hot and cold HCO
897 3 /Na/CO₂-rich Portuguese mineral waters: a review and reinterpretation. *Environmental Geology* 40, 53–63.
898 <https://doi.org/10.1007/s002540000151>.
- 899 Martín-Loeches, M., Pavón-García, J., Molina-Navarro, E., Martínez-Santos, P., Almeida, C., Reyes-López, J.,
900 Cienfuegos-Hevia, I., Sastre-Merlín, A., 2020. Hydrogeochemistry of granitic mountain zones and the influence of
901 adjacent sedimentary basins at their tectonic borders: the case of the Spanish Central System batholith. *Hydrogeol*
902 *J.* <https://doi.org/10.1007/s10040-020-02202-1>.
- 903 Mattei, A., Huneau, F., Garel, E., Santoni, S., Vystavna, Y., 2021. Evaporation in Mediterranean conditions: estimations
904 based on isotopic approaches at the watershed scale. *Hydrological Processes* n/a. <https://doi.org/10.1002/hyp.14085>
- 905 Michard, G., 1990. Behaviour of major elements and some trace elements (Li, Rb, Cs, Sr, Fe, Mn, W, F) in deep hot waters
906 from granitic areas. *Chemical Geology* 89, 117–134.
- 907 Mikhail, S., Sverjensky, D.A., 2014. Nitrogen speciation in upper mantle fluids and the origin of Earth's nitrogen-rich
908 atmosphere. *Nature Geoscience* 7, 816–819. <https://doi.org/10.1038/ngeo2271>.
- 909 Minissale, A., 2004. Origin, transport and discharge of CO₂ in central Italy. *Earth-Science Reviews* 66, 89–141.
910 <https://doi.org/10.1016/j.earscirev.2003.09.001>.
- 911 Minissale, A., Donato, A., Procesi, M., Pizzino, L., Giammanco, S., 2019. Systematic review of geochemical data from
912 thermal springs, gas vents and fumaroles of Southern Italy for geothermal favourability mapping. *Earth-Science*
913 *Reviews* 188, 514–535. <https://doi.org/10.1016/j.earscirev.2018.09.008>.
- 914 Minissale, A., Magro, G., Martinelli, G., Vaselli, O., Tassi, G.F., 2000. Fluid geochemical transect in the Northern
915 Apennines (central-northern Italy): fluid genesis and migration and tectonic implications. *Tectonophysics* 319, 199–
916 222. [https://doi.org/10.1016/S0040-1951\(00\)00031-7](https://doi.org/10.1016/S0040-1951(00)00031-7).
- 917 Minissale, A., Magro, G., Tassi, F., Frau, F., Vaselli, O., 1999. The origin of natural gas emissions from Sardinia island,
918 Italy. *Geochemical journal* 33, 1–12.
- 919 Moritz, A., Hélie, J.-F., Pinti, D.L., Larocque, M., Barnetche, D., Retailleau, S., Lefebvre, R., Gélinas, Y., 2015. Methane
920 Baseline Concentrations and Sources in Shallow Aquifers from the Shale Gas-Prone Region of the St. Lawrence
921 Lowlands (Quebec, Canada). *Environ. Sci. Technol.* 49, 4765–4771. <https://doi.org/10.1021/acs.est.5b00443>.
- 922 Mörner, N.-A., Etiopie, G., 2002. Carbon degassing from the lithosphere. *Global and Planetary Change* 33, 185–203.
- 923 Nlend, B., Huneau, F., Garel, E., Santoni, S., Mattei, A., 2023. Precipitation isoscapes in areas with complex topography:
924 Influence of large-scale atmospheric dynamics versus microclimatic phenomena. *Journal of Hydrology* 617, 128896.
925 <https://doi.org/10.1016/j.jhydrol.2022.128896>.
- 926 Paternoster, M., Oggiano, G., Sinisi, R., Caracausi, A., Mongelli, G., 2017. Geochemistry of two contrasting deep fluids
927 in the Sardinia microplate (western Mediterranean): Relationships with tectonics and heat sources. *Journal of*
928 *Volcanology and Geothermal Research* 336, 108–117. <https://doi.org/10.1016/j.jvolgeores.2017.02.011>.

- 929 Paull, C., Lorenson, T., Borowski, W., Ussler, B., Olsen, K., Rodriguez, N., 2000. Isotopic composition of CH₄, CO₂
930 species, and sedimentary organic matter within samples from the Blake Ridge: Gas source implications. Proceedings
931 of the Ocean Drilling Program: Scientific Results 164. <https://doi.org/10.2973/odp.proc.sr.164.207.2000>.
- 932 Penna, D., Stenni, B., Šanda, M., Wrede, S., Bogaard, T. A., Gobbi, A., Borga, M., Fischer, B. M. C., Bonazza, M., and
933 Chárová, Z., 2010. On the reproducibility and repeatability of laser absorption spectroscopy measurements for δ²H
934 and δ¹⁸O isotopic analysis, *Hydrol. Earth Syst. Sci.*, 14, 1551–1566, <https://doi.org/10.5194/hess-14-1551-2010>.
- 935 Petrović, T., Zlokolica-Mandić, M., Veljković, N., Vidojević, D., 2010. Hydrogeological conditions for the forming and
936 quality of mineral waters in Serbia. *Journal of Geochemical Exploration* 107, 373–381.
- 937 Piccoli, F., Vitale Brovarone, A., Ague, J.J., 2018. Field and petrological study of metasomatism and high-pressure
938 carbonation from lawsonite eclogite-facies terrains, Alpine Corsica. *Lithos* 304–307, 16–37.
939 <https://doi.org/10.1016/j.lithos.2018.01.026>.
- 940 Powell, T., Cumming, W., 2010. Spreadsheets for geothermal water and gas geochemistry, in: Proceedings. pp. 1–3.
- 941 Ravna, E.J.K., Andersen, T.B., Jolivet, L., Capitani, C.D., 2010. Cold subduction and the formation of lawsonite eclogite
942 – constraints from prograde evolution of eclogitized pillow lava from Corsica. *Journal of Metamorphic Geology* 28,
943 381–395. <https://doi.org/10.1111/j.1525-1314.2010.00870.x>.
- 944 Rojey, A., 1997. Technological innovations in gas field operations; L'innovation technique dans l'exploitation des
945 ressources gazières. *Gaz d'Aujourd'hui* (Paris), 121 : 404-407, ISSN : 0016-5328.
- 946 Rome, S., Giorgetti, J.-P., 2007. Corsican mountains and its climatic features [WWW Document]. URL
947 <https://doi.org/10.4267/2042/14846>.
- 948 Rossi, P., Cocherie, A., Fanning, C.M., 2015. Evidence in Variscan Corsica of a brief and voluminous Late Carboniferous
949 to Early Permian volcanic-plutonic event contemporaneous with a high-temperature/low-pressure metamorphic
950 peak in the lower crust. *Bulletin de la Société Géologique de France* 186, 171–192.
- 951 Ruzié, L., Aubaud, C., Moreira, M., Agrinier, P., Dessert, C., Gréau, C., Crispi, O., 2013. Carbon and helium isotopes in
952 thermal springs of La Soufrière volcano (Guadeloupe, Lesser Antilles): implications for volcanological monitoring.
953 *Chemical Geology* 359, 70–80.
- 954 Sacchi, E., Cuoco, E., Oster, H., Paolucci, V., Tedesco, D., Viaroli, S., 2022. Tracing groundwater circulation in a valuable
955 mineral water basin with geochemical and isotopic tools: the case of FERRARELLE, Riardo basin, Southern Italy.
956 *Environ Geochem Health* 44, 1–28. <https://doi.org/10.1007/s10653-021-00845-x>.
- 957 Serrano, O., Allanic, C., Magar, M., 2013. Synthèse géologique du bassin tertiaire de la Plaine orientale Corse - Liaison
958 Terre-Mer entre San Nicolao et Solenzara (Rapport final No. BRGM/RP-62303-FR).
- 959 Sherwood Lollar, B., Westgate, T.D., Ward, J.A., Slater, G.F., Lacrampe-Couloume, G., 2002. Abiogenic formation of
960 alkanes in the Earth's crust as a minor source for global hydrocarbon reservoirs. *Nature* 416, 522–524.
961 <https://doi.org/10.1038/416522a>.
- 962 Štrbački, J., Živanović, V., Čuk Đurović, M., Atanacković, N., Dragišić, V., 2020. Origin, diversity and geothermal
963 potentiality of thermal and mineral waters in Vrnjačka Banja, Serbia. *Environ Earth Sci* 79, 309.
964 <https://doi.org/10.1007/s12665-020-09050-y>.
- 965 Tarvainen, T., Sapon, S., Jarva, J., 2019. Applying heatmaps in interpretation of geochemical baseline data on urban soils
966 in Finland. *Journal of Geochemical Exploration* 205, 106345. <https://doi.org/10.1016/j.gexplo.2019.106345>

- 967 Tassi, F., Feyzullayev, A.A., Bonini, M., Sani, F., Aliyev, C.S., Darrah, T.H., Vaselli, O., Baghirli, R.J., 2020. Mantle vs.
968 crustal fluid sources in the gas discharges from Lesser Caucasus and Talysh Mountains (Azerbaijan) in relation to
969 the regional geotectonic setting. *Applied Geochemistry* 118, 104643.
970 <https://doi.org/10.1016/j.apgeochem.2020.104643>.
- 971 Thatcher, L.L., Janzer, V.J., Edwards, K.W., 1977. *Methods for Determination of Radioactive Substances in Water and*
972 *Fluvial Sediments*. U.S. Government Printing Office.
- 973 Thiébaud, E., Dzikowski, M., Gasquet, D., Renac, C., 2010. Reconstruction of groundwater flows and chemical water
974 evolution in an amagmatic hydrothermal system (La Léchère, French Alps). *Journal of Hydrology* 381, 189–202.
975 <https://doi.org/10.1016/j.jhydrol.2009.11.041>.
- 976 Vitale Brovarone, A., Beyssac, O., Malavieille, J., Molli, G., Beltrando, M., Compagnoni, R., 2013. Stacking and
977 metamorphism of continuous segments of subducted lithosphere in a high-pressure wedge: The example of Alpine
978 Corsica (France). *Earth-Science Reviews* 116, 35–56. <https://doi.org/10.1016/j.earscirev.2012.10.003>
- 979 Werner, C., C. I. Schipper, S. J. Cronin, P. H. Barry, and M. K. Stewart. 2022. 'Magmatic Carbon and Helium in Springs
980 Reveals the Vitality of a Dormant Volcano, Taranaki, New Zealand'. *Geophysical Research Letters* 49 (18):
981 e2022GL099273. <https://doi.org/10.1029/2022GL099273>.
- 982 Whiticar, M.J., Faber, E., Schoell, M., 1986. Biogenic methane formation in marine and freshwater environments: CO₂
983 reduction vs. acetate fermentation—Isotope evidence. *Geochimica et Cosmochimica Acta* 50, 693–709.
984 [https://doi.org/10.1016/0016-7037\(86\)90346-7](https://doi.org/10.1016/0016-7037(86)90346-7).
- 985 Zippa, E., Plyusnin, A., Shvartsev, S., 2019. The chemical and isotopic compositions of thermal waters and gases in the
986 Republic of Buryatia, Russia. *E3S Web Conf.* 98, 01055. <https://doi.org/10.1051/e3sconf/20199801055>.

Tables

Table 1: Information about sites, springs localities, code name, type and altitude.

Journal Pre-proofs

Spring name	CODE	Type	Geographic Coordinates			
			Altitude (m asl)	in " Lambert 93"		Municipality
				X (m)	Y (m)	
Acqua Acetosa	ACQ	Spring	47	1,227,704.289	6,119,785.550	<i>Serra di Fiumorbo</i>
Caldaniccia Travu	CALD	Spring	284	1,220,620.598	6,111,725.565	<i>Chisa</i>
Vignola Travu	VIGN	Spring	190	1,223,000.993	6,112,347.655	<i>Chisa</i>
Fontanella	FONT	Spring	1	1,231,781.421	6,107,000.355	<i>Solaro</i>
Pietrapola	P-MUR3	Spring	190	1,222,833.837	6,119,744.012	<i>Isolaccio-di-Fiumorbo</i>
	P-LAV	Spring				
	P-LEC	Spring				
	P-LUC	Spring				
	P-MUR1	Spring				
	P-ESC	Spring				
	P-RAST	Spring				

	P-SOA	Spring				
Campo-Favajo	CAM-F	Spring	25	1,231,884.619	6,137,973.405	<i>Antisanti</i>
Puzzichellu	PUZ-F	Borehole	60	1,230,383.109	6,135,227.581	<i>Aghione</i>
	PUZ-N	Spring				
	PUZ-G	Spring				
Fajo-Quarcio	QUAR-D	Spring	110	1,228,744.504	6,142,058.466	<i>Giuncaggio</i>
	QUAR-G	Spring	110			
Vadina	VAD	Spring	18	1,234,334.584	6,129,574.738	<i>Ghisonaccia</i>
Pardina	PARD	Spring	554	1,228,492.188	6,158,708.617	<i>Tarrano</i>
Moita	MOIT	Spring	442	1,228,931.829	6,152,106.468	<i>Moita</i>
Forcione	FORC	Spring	177	1,227,838.685	6,169,146.731	<i>Scata</i>
La Porta	PORT	Spring	369	1,223,782.856	6,169,454.126	<i>Poggio Marinaccio</i>
Piana	PIAN	Spring	370	1,225,496.502	6,164,172.761	<i>Stazzona</i>
Surgente Sottana	SSOT	Borehole	415	1,225,544.676	6,163,060.865	<i>Rappaggio</i>

Surgente Supprana	SSUP	Spring	477	1,225,594.7 39	6,163,049.7 61	<i>Rappaggio</i>
Caldane d'Ampugnani	AMPU	Spring	159	1,229,540.9 88	6,168,923.5 34	<i>San Gavino d'Ampugnani</i>

Journal Pre-proofs

Table 2: Field parameters, hydrochemical and isotopic content of thermo-mineral groundwaters.

SPRINGS CODE	DATE	T.	pH	E.C.	Eh	O ₂	HCO ₃ ⁻	CO ₃ ²⁻	NH ₄	3H	² H	¹⁸ O	Estimated recharge altitude (m.a.s.l.)					
		°C	-	µS/cm ²	mV	mg/L	%	mg/L	mg/L	mg/L	TU	STD	‰	STD	‰	STD	Ave.	STD
ACQ	Apr-18	15.7	5.93	2150	310	0.85	8.7	1437	1.3E-03	0.27			-40.03	0.10	-7.22	0.03	263	34
	Dec-18	17.9	6.01	2120	228	0.28	2.9	1291	1.4E-03	0.08	1.1	0.2	-38.69	0.38	-6.88	0.00		
AMPU	Apr-18	13.5	5.99	1126	319	3.85	37.9	798	8.3E-04				-43.52	0.09	-7.63	0.05	458	32
	Sep-18	15.7	5.96	1432	338	2.49	25.1	937	9.1E-04	2.17	1.7	0.2	-44.56	0.14	-8.08	0.06		
	Dec-18	12.9	5.83	1237	356	3.40	32.8	836	6.0E-04	1.63				-43.04	0.34	-7.86		
CALD	Apr-18	33	9.58	150	2	2.11	0.3	63	2.6E-01	1.59			-52.11	0.07	-8.17	0.02	1035	115
CAM-F	Apr-18	16.5	7.83	1405	196	0.25	2.5	468	3.4E-02				-39.64	0.27	-7.13	0.04	228	17
	Sep-18	17.1	7.78	1429	-90	0.01	0.1	494	3.2E-02		0.0		-39.21	0.24	-7.05	0.05		
	Dec-18	16.6	7.67	1381	-111	0.16	1.6	461	2.3E-02				-39.05	0.10	-6.83	0.16		
FAJO-D	Apr-18	15.7	7.35	698	-25	25.00	2.45	503	1.3E-02				-41.18	0.18	-7.44	0.02	292	35

	Sep-18	16.8	7.03	693	67	-	-	538	6.1E-03	1.3	0.2	-41.30	0.50	-7.37	0.03		
	Dec-18	16.2	7.11	700	-4	2.34	22.9	405	5.5E-03			-39.79	0.34	-7.19	0.09		
	Apr-18	15.5	7.30	704	-34	28.60	2.81	438	9.3E-03			-40.69	0.56	-7.26	0.04		
FAJO-G	Sep-18	16.7	7.16	694	39	-	-	400	6.2E-03	1.1	0.2	-41.19	0.69	-7.51	0.12	277	25
	Dec-18	16.3	7.02	711	9	1.90	19.5	372	4.1E-03			-39.98	0.14	-7.23	0.07		
	Apr-18	17.5	6.13	12150	190	0.02	0.2	1696	2.4E-03			-41.30	0.47	-7.39	0.04		
FONT	Sep-18	19.5	6.06	12200	222	0.20	2	1764	2.2E-03	1.2	0.2	-42.70	0.55	-7.07	0.03	334	45
	Dec-18	18.9	6.46	12070	178	0.77	8.1	1787	5.5E-03			-41.01	0.12	-6.94	0.02		
	Apr-18	15.2	5.77	1002	275	0.08	0.8	676	4.3E-04			-46.08	0.31	-7.91	0.12		
FORC	Sep-18	15.4	5.79	1026	290	0.75	7.6	665	4.4E-04	0.0		-46.66	0.07	-8.23	0.07	580	17
	Dec-18	15.4	5.80	1022	298	0.17	1.7	689	4.6E-04			-46.03	0.10	-8.23	0.10		
	Apr-18	13.5	5.99	1149	311	0.70	7	781	8.1E-04			-47.40	0.44	-8.37	0.01		
MOIT	Sep-18	14.9	5.89	1216	279	-	-	856	7.1E-04	0.24	0.0	-47.05	0.34	-8.15	0.04	650	24

	Dec-18	13.8	5.99	1010	279	0.52	5.3	694	7.2E-04	0.25			-46.81	0.58	-8.16	0.08		
	Apr-18	12	5.44	516	402	1.52	15.3	265	7.8E-05	0.17			-48.36	0.31	-8.50	0.06		
PARD	Sep-18	12.5	5.53	556	233	0.55	5.6	314	1.1E-04	0.06	2.3	0.3	-48.57	0.40	-8.40	0.02	702	41
	Dec-18	12.1	5.20	497	373	1.61	16	275	4.7E-05	0.01			-47.84	0.40	-8.28	0.02		
	Sep-18	44	8.89	372	-185	0.54		128	1.1E-01		0.0		-54.81	0.30	-9.22	0.06		
P-B	Dec-18	43.2	9.67	338	-61	4.04	67.1	100	5.0E-01				-55.06	0.20	-9.10	0.04	1045	17
	Apr-18	48.6	9.18	336	189	0.53	9.8	122	1.9E-01				-54.65	0.22	-9.09	0.05		
P-LAV	Sep-18	48.9	9.00	376	-174	2.43		118	1.3E-01		0.0		-54.47	0.03	-8.96	0.02	1045	21
	Dec-18	49.9	9.63	340	-123	0.55	9.8	110	4.9E-01	0.56			-55.26	0.28	-9.35	0.07		
	Apr-18	31.3	9.32	334	202	3.89	48.4	110	2.4E-01	0.46			-54.96	0.24	-9.33	0.05		
P-LUC	Sep-18	34.5	9.36	338	19	1.42	20.4	132	3.2E-01	0.32	0.0		-51.63	0.13	-8.62	0.06	1031	43
	Dec-18	32.5	9.60	336	-82	1.17	16.5	109	4.6E-01	0.43			-54.97	0.16	-8.85	0.06		
P-MUR3	Dec-18	50.1	9.38	338	-98	2.06	37.1	112	1.8E-01	0.47			-54.10	0.31	-8.89	0.08	1036	24

	Sep-18	49.7	8.96	378	-182	-	-	116	1.1E-01	0.0	-55.58	0.03	-9.09	0.00			
	Apr-18	49	9.15	337	189	2.33	42.6	118	2.9E-01		-55.20	0.23	-9.17	0.03			
PORT	Apr-18	12.1	6.17	2390	259	1.14	11	1642	2.6E-03		-54.29	0.36	-9.03	0.12	1061	26	
	Sep-18	15.9	5.98	3140	110	0.24	2.6	2102	2.1E-03	0.0	-54.83	0.08	-9.20	0.06			
P-RAST	Sep-18	54.7	8.96	340	-24	0.99	18.1	105	1.0E-01	0.0	-55.19	0.03	-9.21	0.04	1043	17	
	Dec-18	54.2	9.20	340	-147	1.22	22.7	121	2.0E-01		-54.67	0.13	-9.05	0.03			
P-SOA	Apr-18	50.7	9.09	339	188	0.65	11.6	131	1.7E-01		-55.02	0.55	-9.18	0.01			
	Sep-18	50.8	9.16	375	-170	0.06	1.1	133	2.0E-01	1.41	0.0	-54.71	0.49	-9.03	0.07	1047	20
	Dec-18	49.4	9.55	340	-175	0.82	14.5	106	4.0E-01	1.39		-54.68	0.38	-8.79	0.08		
PUZ-F	Apr-18	16.7	7.32	1800	213	6.30	63.4	559	1.2E-02		-38.65	0.59	-6.70	0.05			
	Sep-18	16.9	7.10	1048	18	0.12	1.2	498	6.6E-03	1.3	0.2	-38.55	0.26	-7.07	0.06	199	14
	Dec-18	16.7	7.17	1052	-125	0.24	2.5	492	7.8E-03			-38.28	0.21	-6.92	0.04		
PUZ-N	Apr-18	14.2	6.96	1309	214	1.60	16.2	559	5.4E-03	0.25		-38.13	0.31	-6.81	0.03	163	29

	Sep-18	17.5	7.05	1592	-107	1.14	11.4	616	7.4E-03	0.29	0.0	-38.81	0.81	-7.18	0.07			
	Dec-18	15.5	6.96	1325	-119	1.49	14.9	577	5.6E-03	0.12		-38.00	0.30	-6.88	0.03			
	Apr-18	13.6	5.69	920	302	0.91	9.3	659	3.5E-04	0.11		-49.02	0.45	-8.50	0.09			
S-SOT	Sep-18	13.7	5.72	910	308	0.62	6.2	580	3.2E-04	0.09	1.8	0.2	-50.28	0.22	-8.43	0.05	753	29
	Dec-18	13.7	5.72	962	309	1.09	11.1	628	3.5E-04				-49.06	0.30	-8.43	0.09		
	Apr-18	11.7	4.96	254	281	0.75	0.7	115	1.1E-05				-49.60	0.07	-8.61	0.06		
S-SUP	Sep-18	12.5	4.96	257	272	0.02	0.2	83	8.1E-06		1.2	0.2	-49.61	0.15	-8.48	0.03	780	20
	Dec-18	12.2	4.88	255	217	0.01	0.1	98	7.9E-06				-50.01	0.13	-8.54	0.07		
	Apr-18	27.7	7.51	2.89	0	2.63	34	67	2.3E-03	0.34			-55.19	0.18	-9.38	0.05		
VIGN	Sep-18	28.7	8.03	2880	49	2.00	26.1	29	3.3E-03	1.56			-51.63	0.19	-8.77	0.11	876	103
	Dec-18	28	7.47	2870	-20	2.57	33.5	110	3.4E-03				-52.00	0.32	-8.80	0.07		

Table 3: Concentration of dissolved gas sampled with analytical error. Helium and excess air calculation results. (<LOD) limit of detection, (n.m) non-measured, (-) calculation not allowed due to high CO₂ degassing.

SPRING CODE	DATE	CO ₂	He	Ne	H ₂	Ar	O ₂	N ₂	CH ₄	H ₂ S	N ₂ /Ar	He excess	Excess Air
		± 5%	± 3%	± 3%	± 3%	± 3%	± 3%	± 5%	± 3%	± 3%		(EA)	
					mol/L						cm ³ STP/g		
ACQ	Apr-18	2.94E-02	5.90E-09	1.79E-09	<LOD	3.42E-06	8.84E-07	1.16E-04	6.38E-07	<LOD	34	-	-
ACQ	Dec-18	3.60E-02	n.m	8.89E-10	<LOD	4.59E-07	1.44E-06	3.84E-05	2.49E-07	<LOD	84	-	-
S-SOT	Apr-18	5.61E-02	3.69E-09	1.17E-09	<LOD	5.24E-06	3.75E-07	1.85E-04	5.33E-07	3.03E-07	35	-	-
S-SOT	Sept-18	3.59E-02	n.m	2.71E-09	<LOD	4.91E-06	5.63E-07	1.95E-04	5.96E-07	<LOD	40	-	-
S-SOT	Dec-18	3.89E-02	n.m	<LOD	<LOD	2.08E-06	1.34E-07	7.24E-05	3.10E-07	5.17E-07	35	-	-
S-SUP	Apr-18	5.00E-02	2.76E-10	<LOD	<LOD	1.64E-06	2.27E-07	5.50E-05	2.18E-08	<LOD	33	-	-
S-SUP	Sept-18	2.30E-02	n.m	<LOD	<LOD	3.66E-07	3.18E-07	2.52E-05	0.00E+00	5.65E-07	69	-	-
S-SUP	Dec-18	3.14E-02	n.m	8.16E-10	<LOD	1.08E-06	2.41E-07	4.05E-05	9.10E-08	1.03E-06	38	-	-
AMPU	Apr-18	2.51E-02	3.37E-09	5.47E-09	<LOD	8.40E-06	1.06E-04	2.78E-04	4.76E-08	<LOD	33	-	-
AMPU	Sept-18	1.79E-02	n.m	1.10E-09	<LOD	1.96E-06	3.36E-06	7.82E-05	2.67E-08	<LOD	40	-	-

AMPU	Dec-18	1.99E-02	1.05E-09	3.49E-09	<LOD	7.96E-06	9.51E-05	2.95E-04	3.61E-08	<LOD	37	-	-
FONT	Apr-18	3.37E-02	1.35E-09	1.37E-09	<LOD	1.25E-06	1.10E-07	4.20E-05	9.29E-07	6.77E-08	34	-	-
FONT	Dec-18	2.28E-02	n.m	<LOD	<LOD	3.22E-07	1.92E-07	1.10E-05	3.79E-07	<LOD	34	-	-
FONT	Sept-18	1.95E-02	n.m	3.13E-10	1.84E-08	5.77E-07	1.09E-06	2.20E-05	5.32E-07	<LOD	38	-	-
FORC	Apr-18	3.09E-02	1.26E-08	1.68E-09	<LOD	1.05E-05	1.35E-07	4.17E-04	1.04E-06	<LOD	40	-	-
FORC	Sept-18	1.93E-02	n.m	2.34E-09	<LOD	6.72E-06	4.13E-07	3.01E-04	8.27E-07	<LOD	45	-	-
FORC	Dec-18	2.49E-02	1.89E-08	3.20E-09	<LOD	9.08E-06	4.60E-07	4.23E-04	1.20E-06	6.77E-08	47	-	-
PORT	Apr-18	4.64E-02	n.m	<LOD	<LOD	2.83E-06	2.13E-07	9.52E-05	1.17E-05	<LOD	34	-	-
PORT	Sept-18	3.06E-02	n.m	<LOD	<LOD	8.02E-07	2.81E-06	2.80E-05	5.14E-06	<LOD	35	-	-
PARD	Apr-18	4.45E-02	4.15E-09	2.56E-09	<LOD	3.46E-06	1.82E-05	1.10E-04	1.74E-07	<LOD	32	-	-
CALD	Apr-18	3.50E-06	2.53E-08	7.93E-09	<LOD	1.72E-05	1.24E-05	5.85E-04	2.38E-07	<LOD	34	5.30E-07	-1.10E-03
P-B	Sept-18	1.44E-06	n.m	6.29E-09	<LOD	1.14E-05	1.05E-06	3.89E-04	2.55E-06	1.34E-07	34	-	-1.52E-03
P-B	Dec-18	2.76E-06	7.82E-07	6.09E-09	<LOD	9.23E-06	2.07E-05	3.43E-04	8.70E-07	<LOD	37	1.75E-05	-9.76E-04

P-LAV	Apr-18	7.64E-05	1.15E-07	6.35E-09	8.92E-08	1.47E-05	4.55E-07	4.36E-04	4.08E-06	<LOD	30	2.54E-06	-2.43E-03
P-LAV	Sept-18	8.30E-06	n.m	5.88E-09	<LOD	1.30E-05	1.18E-06	4.51E-04	4.33E-06	1.94E-07	35	-	-2.62E-03
P-LAV	Dec-18	2.26E-05	2.25E-07	6.07E-09	<LOD	1.19E-05	9.04E-07	4.00E-04	3.94E-06	1.09E-07	34	5.02E-06	-1.95E-03
P-SOA	Apr-18	2.27E-05	6.79E-08	8.13E-09	6.58E-07	1.76E-05	6.63E-07	5.45E-04	5.01E-06	<LOD	31	1.48E-06	-9.44E-04
P-SOA	Sept-18	3.10E-06	n.m	5.69E-09	4.55E-10	1.18E-05	2.25E-06	4.18E-04	3.79E-06	6.83E-08	35	-	-2.42E-03
P-SOA	Dec-18	3.69E-05	2.34E-07	6.07E-09	<LOD	1.22E-05	6.10E-07	4.14E-04	4.30E-06	2.29E-07	34	5.22E-06	-2.10E-03
PUZ-F	Apr-18	1.23E-03	2.94E-08	9.52E-09	<LOD	2.01E-05	2.91E-07	7.53E-04	9.58E-04	1.42E-04	38	6.12E-07	3.10E-04
PUZ-F	Sept-18	8.79E-04	n.m	9.35E-09	<LOD	1.63E-05	9.68E-07	6.97E-04	8.81E-04	1.50E-04	43	-	1.28E-03
PUZ-F	Dec-18	9.81E-04	3.15E-08	8.96E-09	<LOD	1.77E-05	2.67E-07	7.57E-04	9.15E-04	1.41E-04	43	6.60E-07	2.33E-04
PUZ-N	Sept-18	1.06E-03	n.m	6.83E-09	<LOD	1.21E-05	2.40E-07	4.81E-04	1.93E-04	1.06E-03	40	-	-9.04E-04
CAM-F	Apr-18	3.55E-04	8.76E-09	2.53E-09	<LOD	8.91E-06	3.61E-07	2.51E-04	1.00E-03	3.12E-05	28	1.87E-07	-6.00E-03
CAM-F	Sept-18	2.40E-04	n.m	2.01E-09	1.33E-08	7.17E-06	2.79E-07	2.26E-04	2.13E-03	4.41E-05	32	-	-6.24E-03
CAM-F	Dec-18	3.10E-04	9.22E-09	3.80E-09	2.17E-08	8.28E-06	2.25E-07	2.84E-04	1.89E-03	3.71E-05	34	1.87E-07	-3.93E-03

Table 4: CFC and SF₆ concentrations measured in water in pmol/L and pptv.

SPRINGS CODE	SF6		CFC-12		CFC-11		CFC-113	
	pmol/L	pptv	pmol/L	pptv	pmol/L	pptv	pmol/L	pptv
FORC	8.39E-04	2.75	1.23E-01	30.23	1.34	88.03	0.00E+00	-
S-SOT	1.65E-03	5.41	6.78E-01	166.82	3.22	211.58	5.88E-02	12.84
P-B	0.00E+00	-	3.14E-01	67.32	4.54	253.58	0.00E+00	-
P-LAV	5.83E-04	1.71	1.11E-01	23.86	2.45	137.02	2.08E-02	3.78
PUZ-F	0.00E+00	-	8.01E-02	19.00	2.27	143.51	8.68E-02	18.27
CAM-F	2.81E-04	0.89	1.95E-01	46.24	4.47	283.04	5.20E-02	10.95
FONT	2.64E-03	8.33	8.03E-02	19.06	2.11	133.45	2.26E-02	4.75

Abstract

The varied gaseous composition of thermo-mineral waters emerging in a non-active zone reflects the diversity and complexity of groundwater pathways and provides important insights into their hydrogeological behaviours. The investigated geochemical content of complex thermo-mineral springs revealed the need to use dissolved gas contents as part of a multi-tracer approach to discriminate processes, geogenic (water-gas-rock interactions), abiotic (geological confinement, flow paths) and biotic activity influencing geochemical of groundwater along regional pathways. Irrespective of the dissolved element content or the water type, examining the overall concentration of dissolved gases enables an effective delineation of regional groundwater flow paths. Using dissolved gas content further contributed to the circumvention of some analytical challenges associated with conventional isotopic or geochemical techniques, often linked to the high concentration of elements such as iron, sulfate, sulfide or other naturally occurring elements content. The primary objectives are to analyse the gas composition of individual springs, to identify the origin of these gases in the groundwater, and to use this gas composition to improve the understanding of the flow patterns contributing to the geochemical diversity observed at the surface of the groundwater. From field investigations in a geologically and structurally complex area of Eastern Corsica (France), three types of gas contents are identified: (type 1) CH₄ & H₂S-rich, (type 2) N₂-rich and (type 3) CO₂-rich. The study of these dissolved gases highlights that the wide geochemical diversity of thermo-mineral waters observed here is not only related to the mineralogical composition of the local aquifer but also involves strong and cumulative interactions along deep regional circulation pathways. This approach also reveals a common deep crustal gaseous influence characterised by N₂ production, which interacts during up flow with groundwater and then with the local metamorphic or sedimentary rock matrix. The groundwater's isotopic and geochemical contents are then altered by local lithologies encountered through both abiotic and biotic interactions. Finally, at shallow depths, phreatic groundwater can add its geochemical and isotopic footprint and dilute this complex mixture before groundwater emerges as mineral spring. This paper answers the primary objectives yet further demonstrates that using dissolved gas as a tracer of groundwater flow paths allows a deeper interpretation of surface geochemical and isotopic observations, distinguishes local from regional flow paths, and provides information about processes at the origin of groundwater diversity.

The combination of tools presented in this paper (i.e., geochemical, dissolved gas, and isotopic tools) allows the establishment of a reliable regional groundwater flow scheme for thermo-mineral waters in a non-active zone. This scheme is essential to improve thermo-mineral water management, and protection to ensure their sustainable quality in front of increasing anthropogenic and climatic pressures.

Keywords

Hydrogeology, thermo-mineral waters, water stable isotopes, water-rock interactions, dissolved gases (CO_2 , CH_4 , H_2S , N_2 , He).

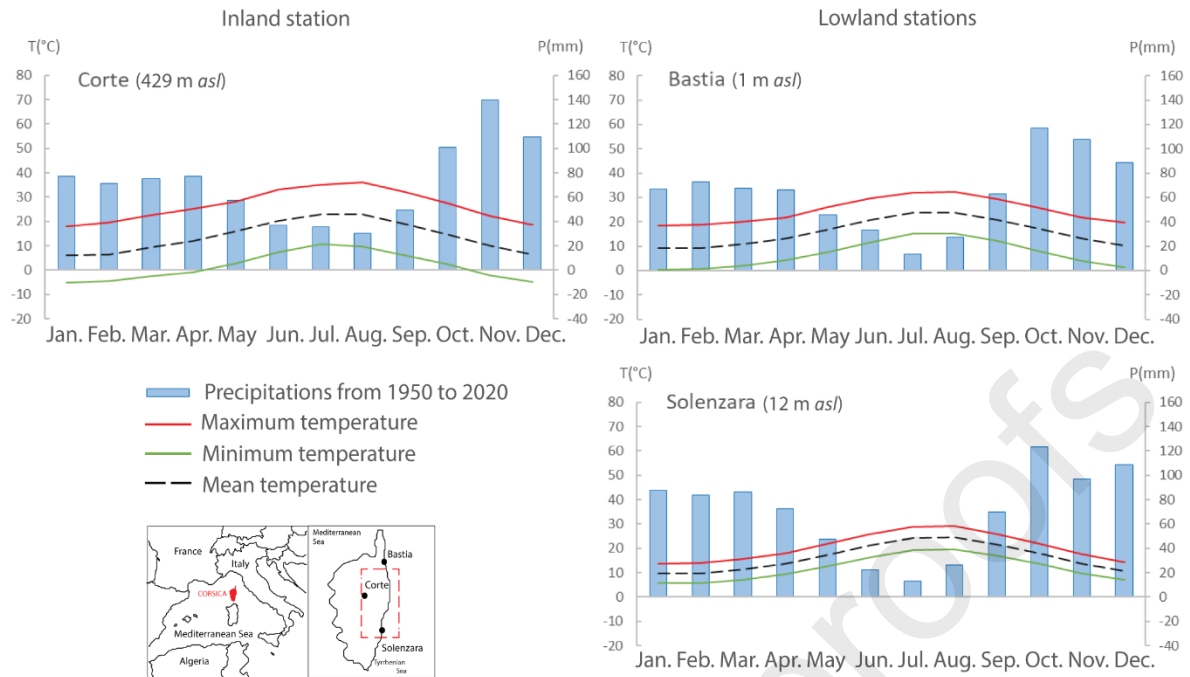
Highlights

- geogenic processes combined with biotic activity generate diversified mineral waters
- CO_2 , N_2 and CH_4 are most widely represented dissolved gases in mineral waters
- excess air can be used as tracer of biotic processes
- complex regional mineral water flows are identified
- an improved regional hydrogeological conceptual model is proposed

Declaration of interests

The authors declare that they have no known competing financial interests or personal relationships that could have appeared to influence the work reported in this paper.

The authors declare the following financial interests/personal relationships which may be considered as potential competing interests:



GEOLOGY

NEOGENE & QUATERNARY

- Quaternary : alluvial deposits
- Miocene : conglomerates

ALPINE OROGENESIS

- Eocene : flyschs
- Undiferenciate deposits from the continental margin
- Ophiolites (pillow lava, gabbro & serpentinite)
- Lustrous Schists :
 - Castagniccia unit - oceanic crust, eclogitic facies
 - Serra di Pigno unit - continental crust, eclogitic facies
 - Inzecca unit - oceanic crust, low blueschist facies

HERCYNIAN OROGENESIS

- Calc-alkaline basic rocks
- Calc-alkaline volcanism
- Alkaline volcanism
- Calc-alkaline granitoids
- Precambrian : gneisses
- Precambrian : micaschists

SYMBOLS

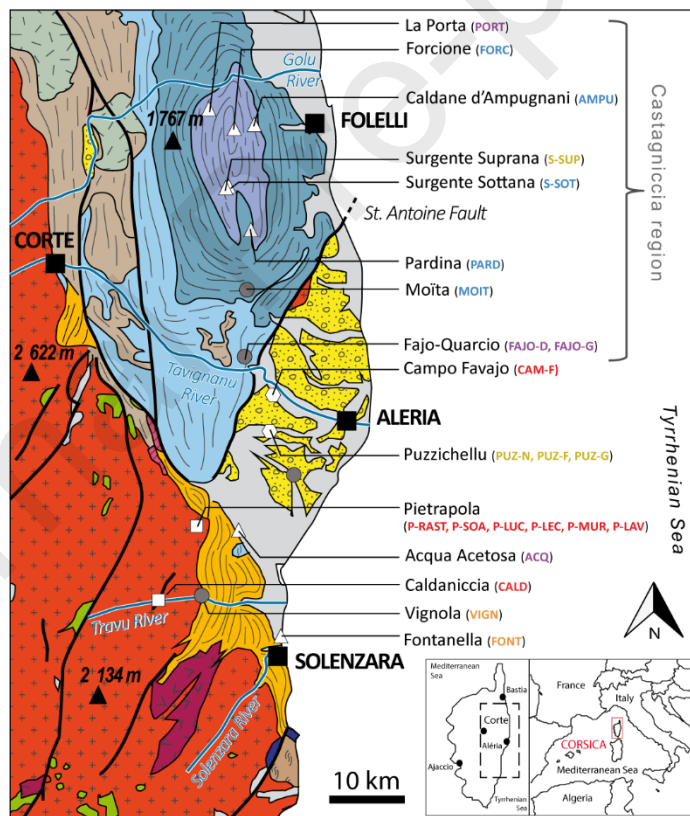
- Fault
- Tectonic contact
- River

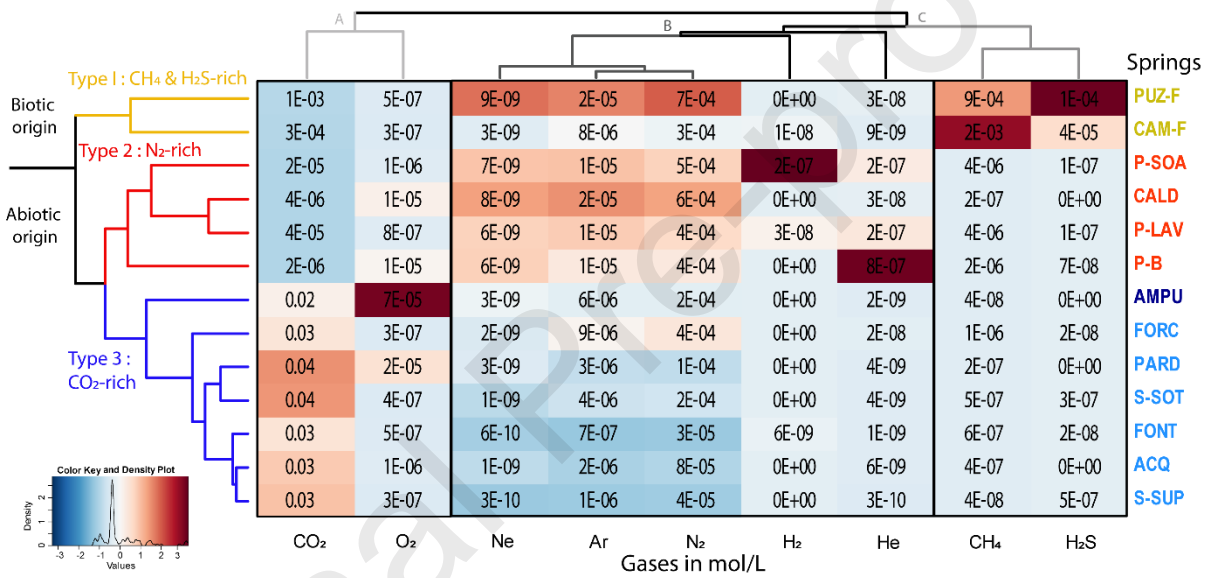
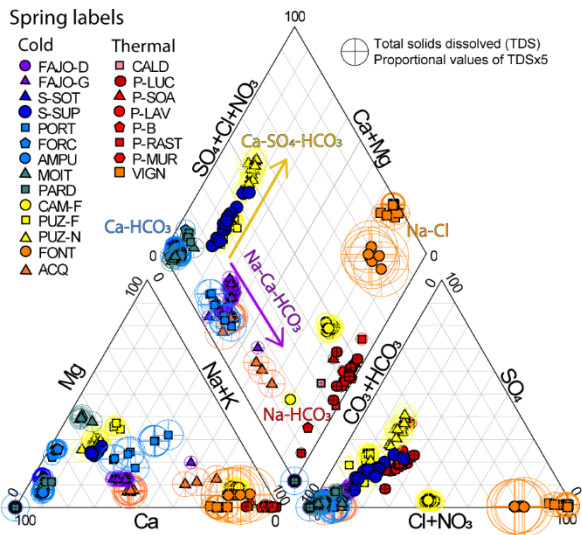
SPRING / GAS TYPE

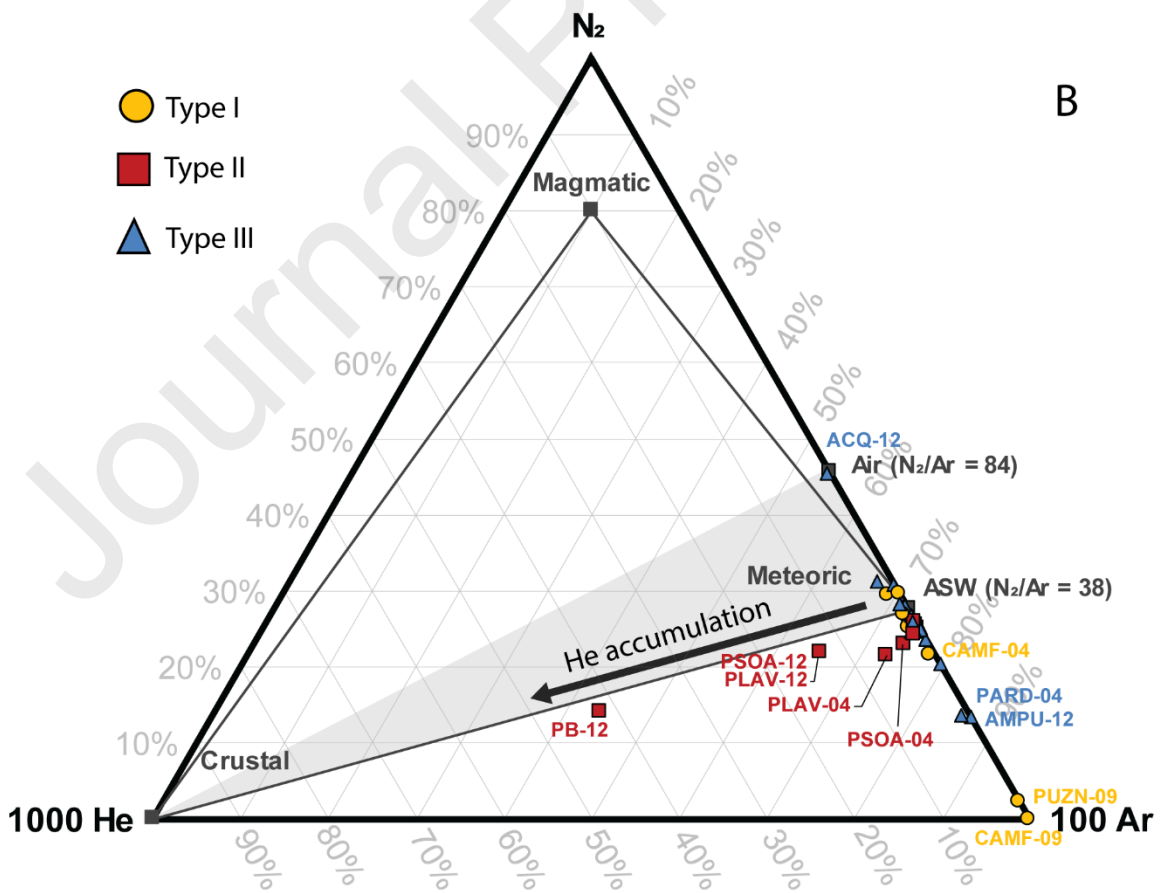
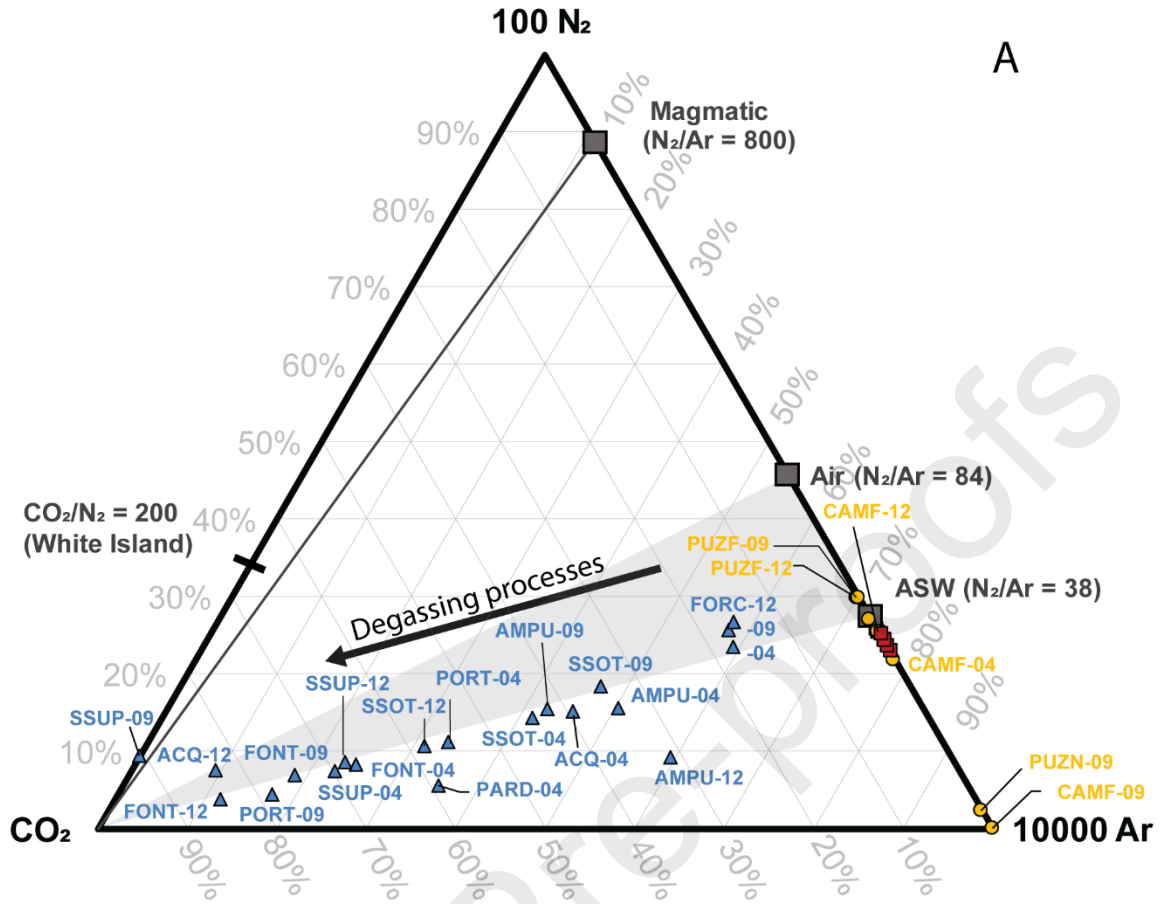
- not measured,
- type I, □ type II, △ type III.

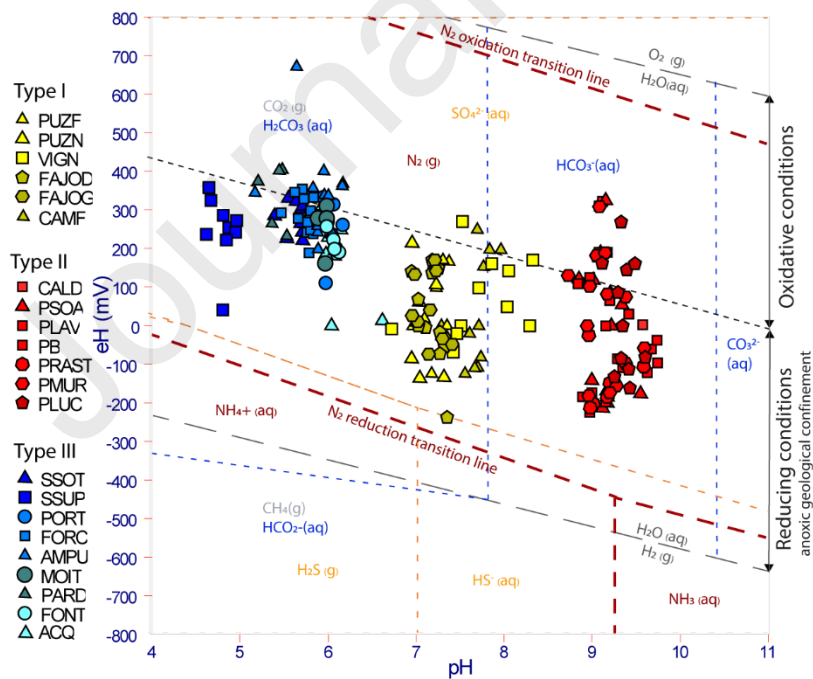
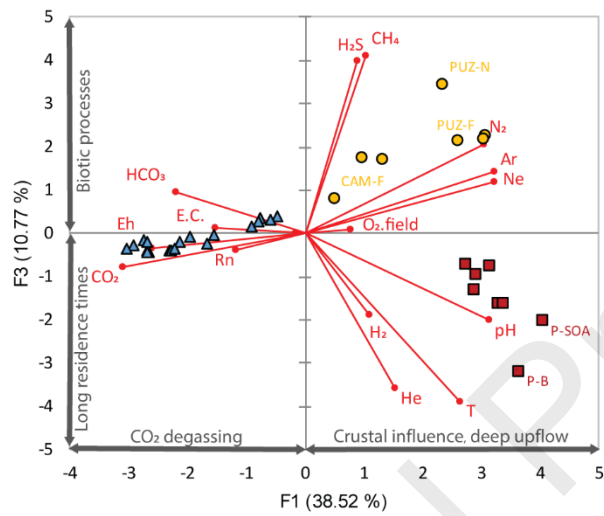
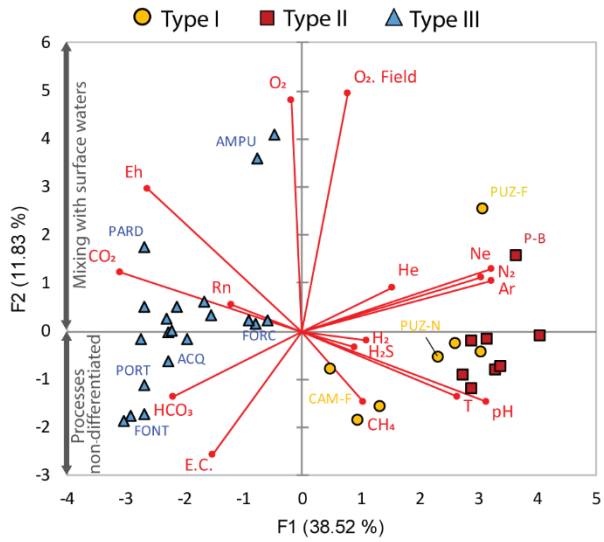
WATER TYPE

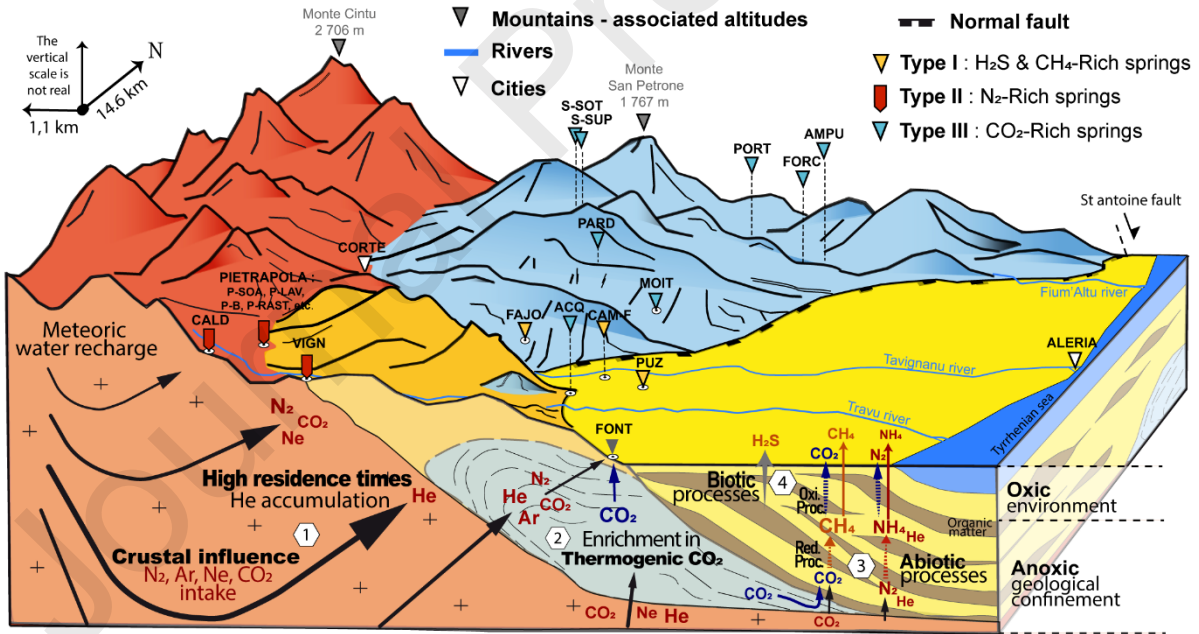
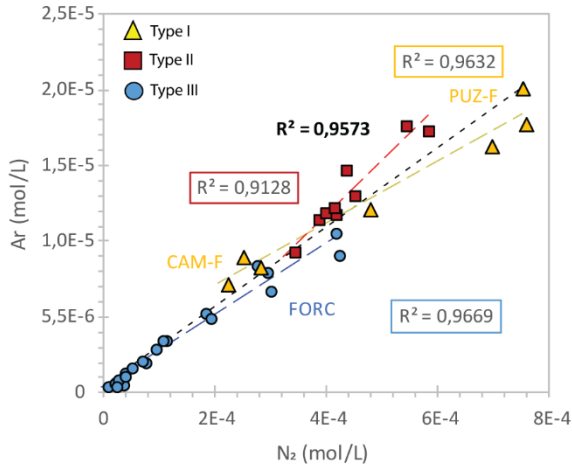
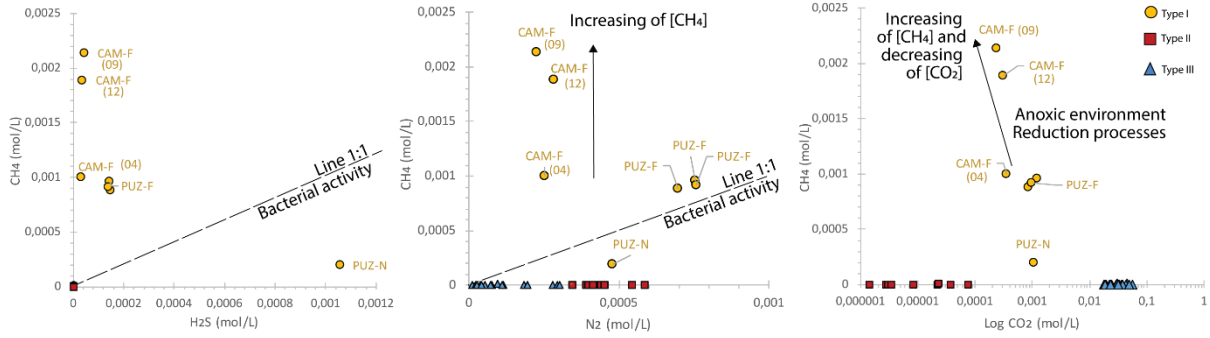
- Ca-HCO₃
- Ca-SO₄-HCO₃
- Na-Cl
- Na-HCO₃
- Na-Ca-HCO₃



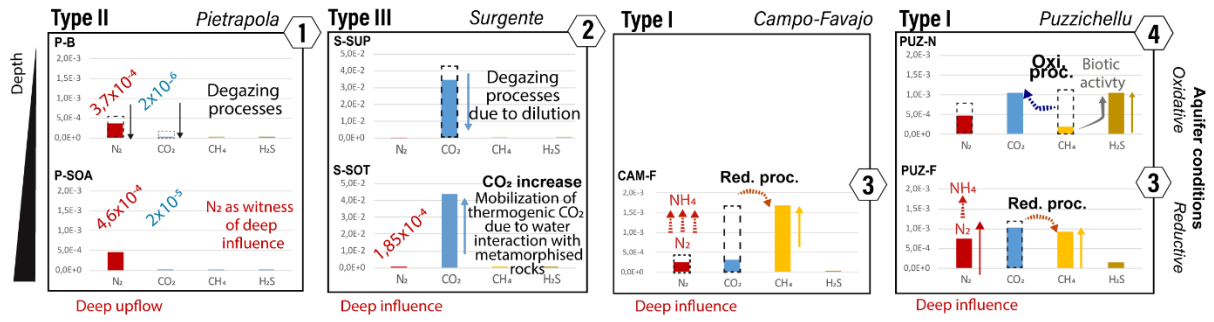








- 1 Crustal influence:** enrichment in N₂, Ar, Ne & CO₂ - Type II
- 2 Thermogenic processes:** enrichment in CO₂ due to re-mobilisation of thermogenic CO₂ according to water interaction with metamorphised rocks - Type III
- 3 Geogenic processes:** Influence of anoxic geological confinement on water, the very reducing aquifer conditions leads to reduce CO₂ into CH₄ and the N₂ into NH₄ - Type I
- 4 Biotic processes:** the bacterial activity in organic matter-rich environment leads to consum CH₄ and sulfate to produce CO₂ and H₂S - Type I



1 **Crustal influence** : enrichment in N₂, Ar, Ne & CO₂ - Type II

2 **Thermogenic processes** : enrichment in CO₂ due to re-mobilisation of thermogenic CO₂ according to water interaction with metamorphosed rocks - Type III

3 **Geogenic processes** : Influence of anoxic geological confinement on water, the very reducing aquifer conditions leads to reduce CO₂ into CH₄ and the N₂ into NH₄ - Type I

4 **Biotic processes** : the bacterial activity in organic matter-rich environment leads to consume CH₄ and sulfate to produce CO₂ and H₂S - Type I

